Reversible Dioxygen Scavenging from Air by a Copper Complex

Kurtis M. Carsch,[†*] Andrei Iliescu,[†*] Ryan D. McGillicuddy,[†] Jarad A. Mason,[†]

Theodore A. Betley[†]

[†]*Department of Chemistry and Chemical Biology*
Harvard University
12 Oxford Street, Cambridge, MA 02138

**These authors contributed equally.*

Corresponding Author: betley@chemistry.harvard.edu

Materials and Methods.

General Considerations. All manipulations were carried out under ambient air in a well-ventilated fume hood, unless specified otherwise. For air-sensitive manipulations, an MBraun inert atmosphere drybox containing either dinitrogen or argon was employed to exclude water and dioxygen. For manipulations in the drybox, all glassware was oven dried at 150 ºC for a minimum of 12 h and cooled in an evacuated antechamber for a minimum of 15 minutes. Benzene, diethyl ether, dichloromethane (DCM), acetonitrile (MeCN), hexanes, pentane, toluene, and tetrahydrofuran (THF) were dried over 4 Å molecular sieves (Strem) prior to use in the drybox. When applicable, solvents were tested with a deep violet solution of sodium benzophenone ketyl in tetrahydrofuran (prepared by stirring 10 mg benzophenone in 10 mL THF with excess metallic sodium for 12 h) to confirm effective oxygen and moisture removal. Chloroform-d_1 was purchased from Cambridge Isotope Labs and stored over anhydrous potassium carbonate for employment under air. Benzene-d_6 and tetrahydrofuran-d_8 were purchased from Cambridge Isotope Labs, degassed, and stored over 4 Å molecular sieves prior to use in the drybox. Reagents potassium graphite (KC_8)[1], $(PPh_3O)_2(H_2O_2)$[2], $(IMes)_2Pd$[3], and $(IMes)_2Pd(O_2)$[3] were synthesized according to literature protocols. Elemental iodine was sublimed prior to use and stored in a freezer with exclusion of light. Reagent 1,2-diphenylhydrazine was crystallized from slow cooling of warm diethyl ether under dinitrogen to ensure removal of trace azoarene. Hydrazine (NH_2NH_2), hydrazine monohydrate ($NH_2NH_2•H_2O$), and 30 % aqueous hydrogen peroxide (H_2O_2) were purchased from Sigma-Aldrich and used as received. (^{EMind}L)Cu(N_2) (**1**) was prepared according to literature procedures[4]. Celite® 545 (J. T. Baker) was dried in a Schlenk flask for 24 h under dynamic vacuum while heating to at least 150 °C prior to use in a drybox. Activated alumina was dried in a Schlenk flask for 48 h under dynamic vacuum at 200 ºC prior to use in a drybox. Silica gel 32-63 μ (AIC, Framingham, MA) was used as received.

Characterization and Physical Measurements.

NMR Spectroscopy. ^{1}H, $^{13}C\{^{1}H\}$, ^{31}P, and ^{19}F NMR spectra were recorded on Varian Unity/Inova 400, 500, or 600 MHz spectrometers. ^{1}H and $^{13}C\{^{1}H\}$ NMR chemical shifts are reported relative to $SiMe_4$ using the chemical shift of residual solvent peaks as reference. ^{19}F NMR chemical shifts are reported relative to an external standard of boron $BF_3(OEt_2)$ (δ –153.00 ppm). ^{31}P NMR chemical shifts are referenced to an external standard of 85 % H_3PO_4 (δ 0.00 ppm). Multiplicity assignments are abbreviated as follows: s = singlet, d = doublet, t = triplet, q = quartet, m = multiplet, br = broad, v. br = very broad.

Resonance Raman Spectroscopy. Resonance Raman measurements were collected at the Center for Nanoscale Systems (CNS) at Harvard University, a member of the National Nanotechnology Coordinated Infrastructure Network (NNCI). Raman spectra were recorded using a Horiba LabRam HR Evolution micro-Raman spectrometer featuring < 1 cm^{-1} spectral resolution and sub-μm spatial resolution for confocal imaging. Measurements were conducted using a 532 nm excitation laser (0.028 mW) at room temperature on solid samples.

Optical Spectroscopy. UV/Visible/NIR spectra were recorded on a Varian Cary 50 UV/Vis spectrometer using air-free quartz cuvettes (0.10 mm path length) and a scan rate of 600 nm/min. Samples were prepared using serial dilution with volumetric glassware to obtain accurate concentrations. Extinction coefficients were determined from a minimum of three concentrations per sample and were calculated by a linear regression fit of the absorbance vs. concentration data.

Electron Paramagnetic Resonance Spectroscopy. EPR spectra were obtained on a Bruker EleXsys E-500 CW-EPR spectrometer. Spectra containing *ca.* 5–10 mg sample were measured as frozen toluene glasses, frozen 2-methyltetrahydrofuran glasses, and/or in solution at a microwave power of 0.6325–2 mW. Effective g-values, g-strain (σ), and hyperfine coupling constants (A) were obtained from spectral simulations of $S = {}^{1}/_{2}$ systems using the program Easyspin.[5]

Electrochemistry. Cyclic voltammetry and differential pulse voltammetry measurements were performed with a CHI660d potentiostat using a three-electrode cell with a glassy carbon working electrode, a platinum wire as the counter electrode, and an $Ag/AgNO_3$ reference electrode. All of the potentials are referenced to the $[Cp_2Fe]^{+/0}$ couple. Saturated tetrabutylammonium hexafluorophosphate ($TBAPF_6$) solutions of 0.2 M in tetrahydrofuran were prepared before each experiment. All measurements were conducted under a dinitrogen atmosphere. No background reaction upon addition of excess $TBAPF_6$ in tetrahydrofuran was observed for all complexes.

Combustion Analysis. Elemental analysis (%CHN) was conducted at Harvard University on a PerkinElmer 2400 Series II CHNS/O Analyzer using bulk recrystallized compounds. Samples were prepared in a dinitrogen-filled drybox, which prevented satisfactory characterization on several complexes due to facile displacement with N_2. In several cases, satisfactory elemental analyses were obtained by considering the presence of solvent molecules intercalated within the unit cell as ascertained by single-crystal X-ray diffraction and ^{1}H NMR spectroscopy.

Metal Complex Syntheses.

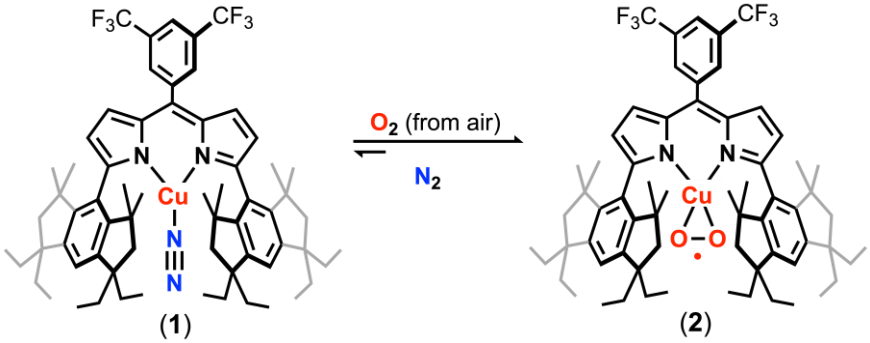

(^{EMind}L)Cu(O_2) (**2**). Crystalline (^{EMind}L)Cu(N_2) (**1**)[4] (0.050 g, 0.046 mmol, 1.0 equiv.) was exported from the dinitrogen-filled drybox and exposed to air, resulting in a rapid color change in the solid state from carrot-orange to Carmine red. The solid was dissolved in hexanes and agitated for 2 minutes to ensure complete oxygenation of the solution. Subsequent removal of solvent *in vacuo* to afford (^{EMind}L)Cu(O_2) (**2**) as an air-stable solid in quantitative yield. Large single crystals suitable for X-ray diffraction were obtained by allowing a concentrated pentane solution of **1** to stand at –10 ºC under air overnight. Large single crystals (> 1 cm^3) could be obtained by adding drops of benzene to the crystallization conditions. ^{1}H NMR (500 MHz, C_6D_6): δ 7.82 (s, 1*H*, fluorinated aryl C–*H*), 7.68 (s, 2*H*, fluorinated aryl C–*H*), 7.12 (s, 2*H*, EMind aryl C–*H*), 6.54 (d, *J* = 4.5 Hz, 2*H*, dipyrrin C–*H*), 6.18 (dd, *J* = 4.2 Hz, 2*H*, dipyrrin C–*H*), 1.90 (d, *J* = 3.9 Hz, 8*H*, EMind aliphatic C–*H*), 1.78 (dt, *J* = 9.3, 6.5 Hz, 8*H*, EMind ethyl C–*H*), 1.61 (apparent heptet from overlapping triplets, *J* = 6.9 Hz, 8*H*, EMind ethyl C–*H*), 1.34 (s, 12*H*, EMind methyl C–*H*), 1.32 (s, 12H, EMind methyl C–*H*), 0.97 (t, *J* = 7.4 Hz, 12*H*, EMind ethyl C–*H*), 0.62 (t, *J* = 7.3 Hz, 12*H*, EMind ethyl C–*H*). ^{13}C{^{1}H} NMR (125 MHz, C_6D_6): δ 162.26, 148.86, 148.59, 141.90, 139.34, 134.76, 131.46, 131.19, 130.93, 130.82, 130.66, 130.41, 128.71, 128.20, 126.32, 125.46, 124.15, 122.45, 121.98, 120.99, 119.81, 52.11, 48.50, 43.93, 34.26, 32.85, 32.50, 31.66, 9.29, 8.62. ^{19}F NMR (470 MHz, C_6D_6): δ –62.27 (s, fluorinated aryl C*F*$_3$). UV/vis (C_6H_{14}) λ_{max}/cm^{-1} (ε/M^{-1} cm^{-1}): 520 (59,000), 490 (21,700), 360 (7,000), 310 (10,000). Anal. Calc. for $C_{65}H_{81}CuF_6N_2O_2$: C 70.98, H 7.42, N 2.55; Found: C 70.95, H 7.11, N 2.47. HRMS (ESI$^+$): *m/z* Calc. 1098.5462 $[C_{65}H_{81}CuF_6N_2O_2]^+$, Found 1098.5493 $[M]^+$.

Note I: Under an atmosphere of N_2 in benzene, trace formation of (^{EMind}L)Cu(C_6H_6) from ^{EMind}L)Cu(O_2) (**2**) is observed (*ca*. 10 %), attributed to an equilibrium favoring dioxygen ligation to the copper center. Nonetheless, air exposure of this mixture affords quantitative conversion to **2**.

Note II: (^{EMind}L)Cu($^{18}O_2$) (**2-$^{18}O_2$**) was prepared by exposure of a degassed J. Young NMR tube containing *in situ* generated (^{EMind}L)Cu(N_2) in C_6D_{12} to an atmosphere of $^{18}O_2$, resulting in effervescence and a color change to red. The contents of the tube were subsequently lyophilized, and Resonance Raman measurements were subsequently conducted on the solid sample without exposure to ambient air, noting facile exchange with $^{16}O_2$ from air, supported by independent Resonance Raman measurements. Due to facile $^{16}O_2$/$^{18}O_2$ exchange under air, HRMS on **2-$^{18}O_2$** was not conducted.

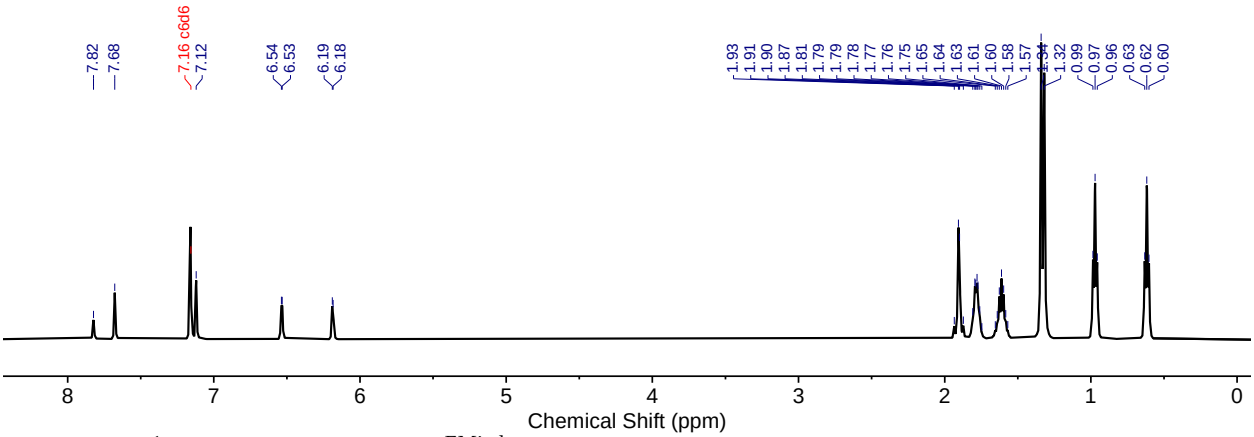

Figure S1. ^{1}H NMR spectrum of (^{EMind}L)Cu(O_2) (**2**), (500 MHz, C_6D_6).

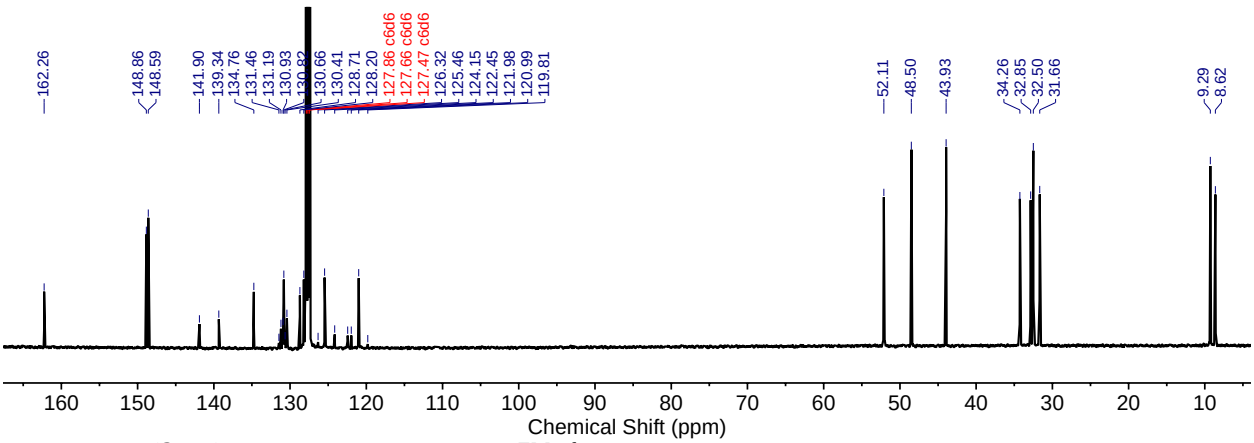

Figure S2. ^{13}C{^{1}H} NMR spectrum of (^{EMind}L)Cu(O_2) (**2**), (125 MHz, C_6D_6).

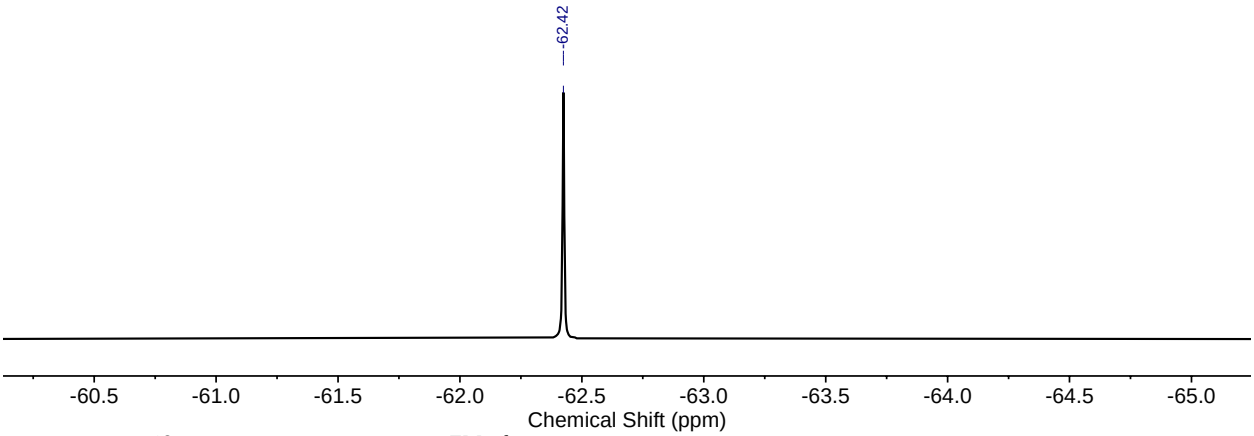

Figure S3. ^{19}F NMR spectrum of (^{EMind}L)Cu(O_2) (**2**), (470 MHz, C_6D_6).

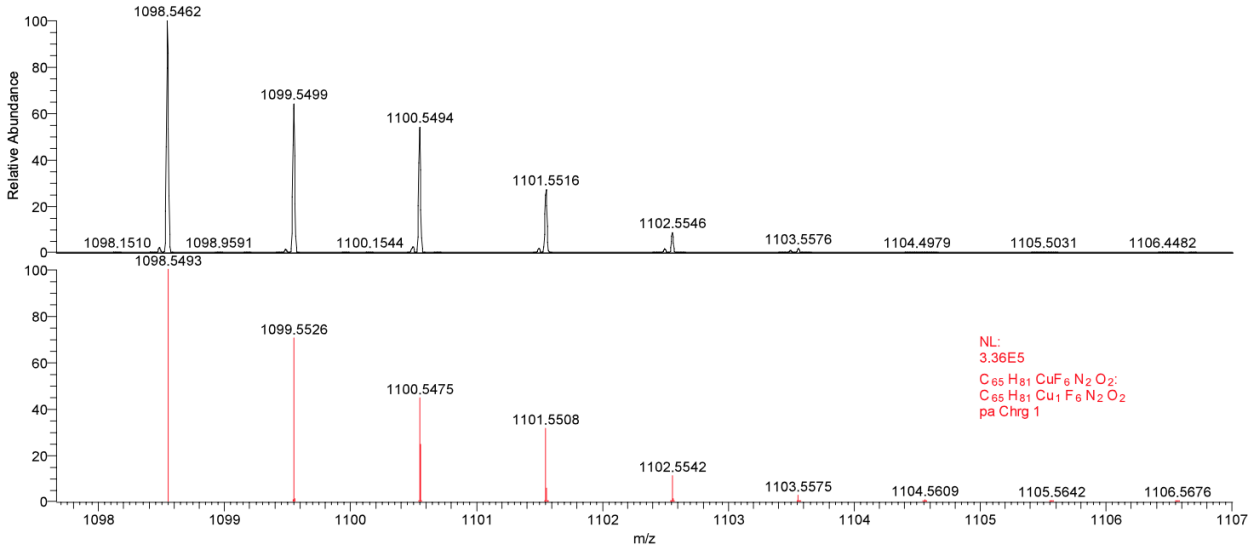

Figure S4. High-resolution mass spectrum of (^{EMind}L)Cu(O_2) (**2**) (*top*, *black*) with simulation (*bottom*, *red*), revealing the expected isotopic pattern.

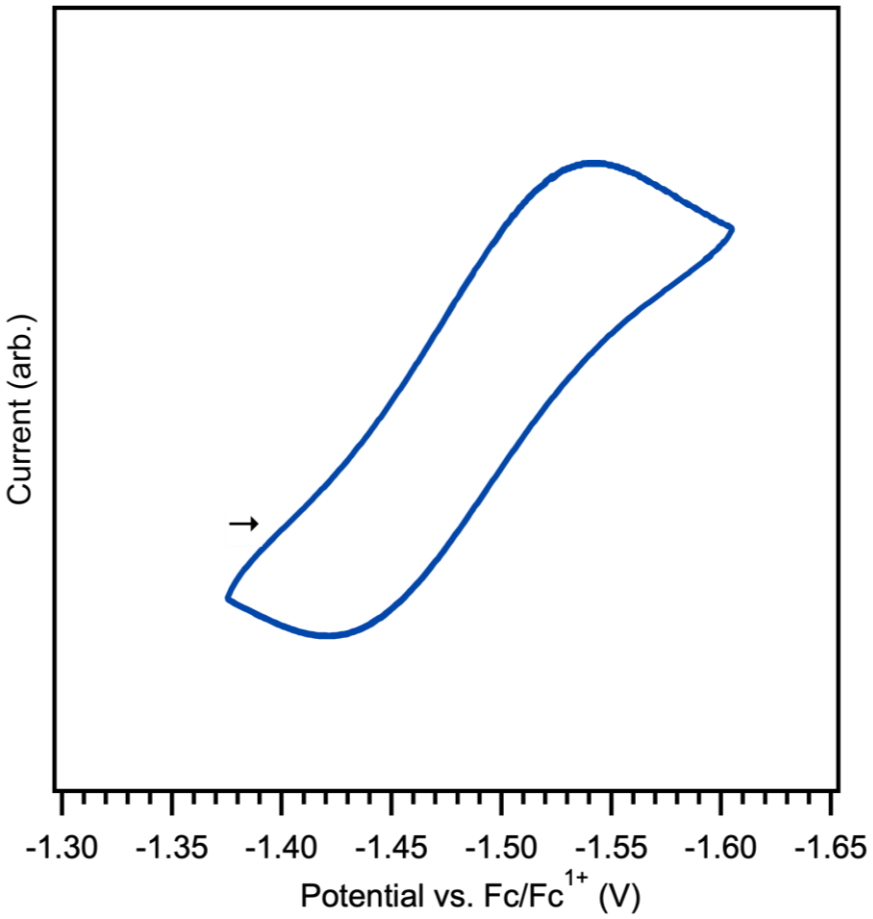

Figure S5. Quasi-reversible one-electron reduction of (^{EMind}L)Cu(O_2) (**2**), ($E_{1/2}$ = –1.48 V vs. Fc/Fc^{1+}) at a scan rate of 100 mV s^{-1}. The data was recorded in 1,2-difluorobenzene under N_2 at a concentration of ca. 0.01 mM, with glassy carbon, Pt-wire, and Ag-wire as the working, counter, and reference electrodes, respectively. Arrows denote initial scan direction. Saturated tetrabutylammonium hexafluorophosphate ([^{n}Bu$_4$N][PF_6]) solutions of 0.2 M in 1,2-difluorobenzene were prepared before each experiment in the presence of molecular sieves to remove trace water. No background reaction between **2** and the electrolyte was observed.

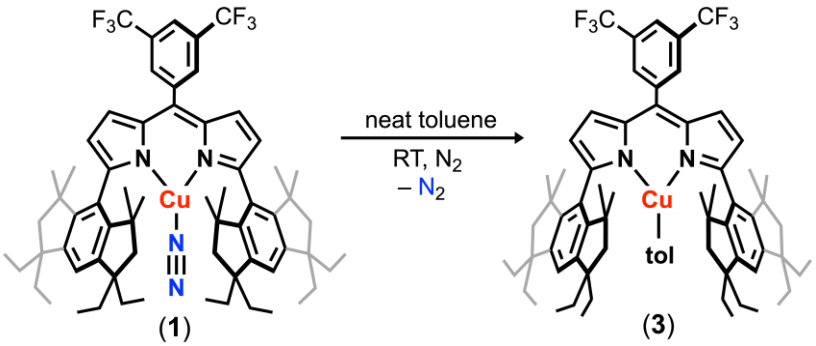

(^EMind^L)Cu(toluene) (**3**). In a dinitrogen-filled drybox, dissolution of (^EMind^L)Cu(N_2) (**1**)[4] (0.050 g, 0.046 mmol, 1.0 equiv.) in toluene (1 mL) afforded rapid effervescence with a color change to red-orange. The mixture was agitated for 30 seconds, followed by removal of solvent *in vacuo* to afford (^EMind^L)Cu(toluene) (**3**) in quantitative yield. ^{1}H NMR (500 MHz, C_7D_8): δ 7.85 (s, 1*H*, fluorinated aryl C–*H*), 7.75 (s, 1*H*, fluorinated aryl C–*H*), 7.05 (s, 2*H*, EMind aryl C–*H*), 6.50 (d, *J* = 4.1 Hz, 2*H*, dipyrrin C–*H*), 6.25 (d, *J* = 4.4 Hz, 2*H*, dipyrrin C–*H*), 1.85 (s, 8*H*, EMind aliphatic C–*H*), 1.74 (dt, *J* = 9.7, 6.8 Hz, 8*H*, EMind ethyl C–*H*), 1.57 (ddp, *J* = 21.2, 14.3, 7.2 Hz, 8*H*, EMind ethyl C–*H*), 1.30 (s, 12*H*, EMind methyl C–*H*), 1.24 (s, 12*H*, EMind methyl C–*H*), 0.95 (t, *J* = 7.3 Hz, 9*H*, EMind ethyl C–*H*), 0.87 (t, *J* = 7.1 Hz, 3*H*, EMind ethyl C–*H*), 0.56 (t, *J* = 7.2 Hz, 12*H*, EMind ethyl C–*H*). ^{13}C{^{1}H} NMR (100 MHz, C_7D_8): δ 159.48, 148.52, 148.45, 143.90, 142.98, 139.47, 137.16, 131.61, 130.98, 130.79, 130.65, 130.32, 130.04, 127.83, 127.59, 127.35, 124.97, 124.73, 124.49, 122.17, 121.27, 120.23, 119.45, 54.19, 47.77, 43.92, 34.20, 32.48, 32.26, 31.53, 22.46, 13.94, 9.06, 9.02. ^{19}F NMR (470 MHz, C_7D_8): δ –62.08 (s, fluorinated aryl C*F*$_3$). A satisfactory elemental analysis of **3** could not be obtained due to the instability of the complex in the absence of excess toluene under an N_2 atmosphere.

Note I: The synthesis of (^EMind^L)Cu(toluene) (**3**) may be performed in air by dissolution of (^EMind^L)Cu(O_2) (**2**) in neat toluene, as confirmed by multinuclear NMR spectroscopy. Nonetheless, we note that removal of excess toluene in the presence of trace dioxygen re-affords majority formation of **2**.

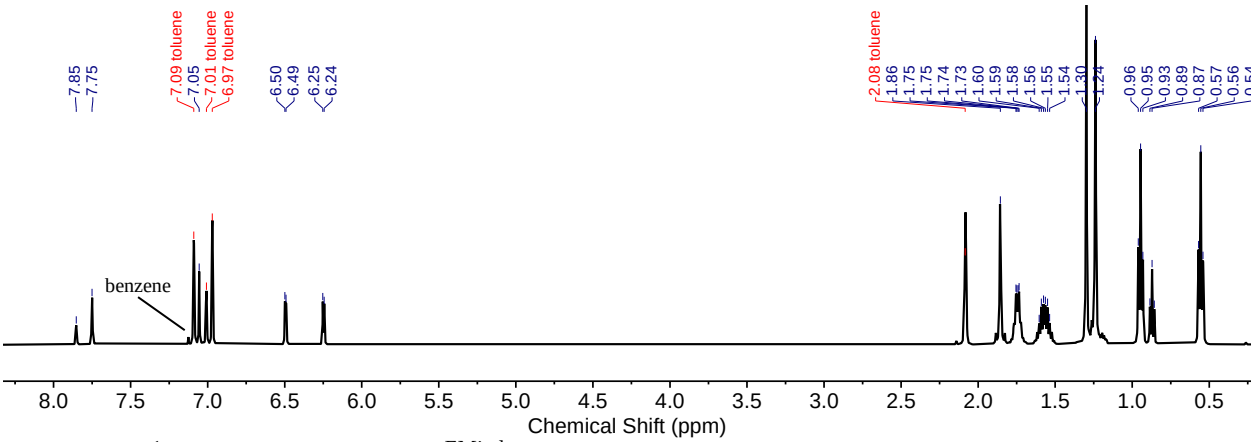

Figure S6. ^{1}H NMR spectrum of (^{EMind}L)Cu(toluene) (**3**), (500 MHz, C_6D_6).

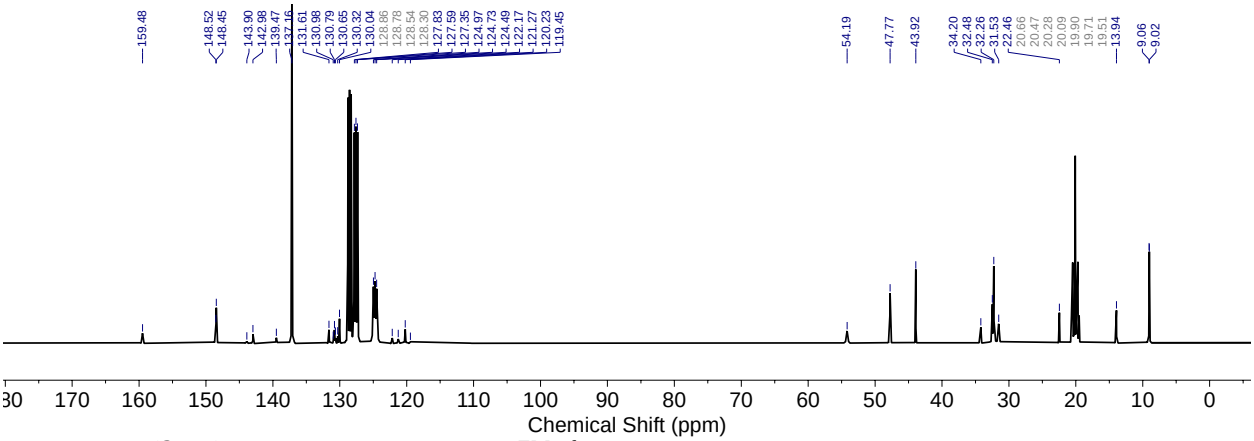

Figure S7. ^{13}C{^{1}H} NMR spectrum of (^{EMind}L)Cu(toluene) (**3**), (100 MHz, C_7D_8).

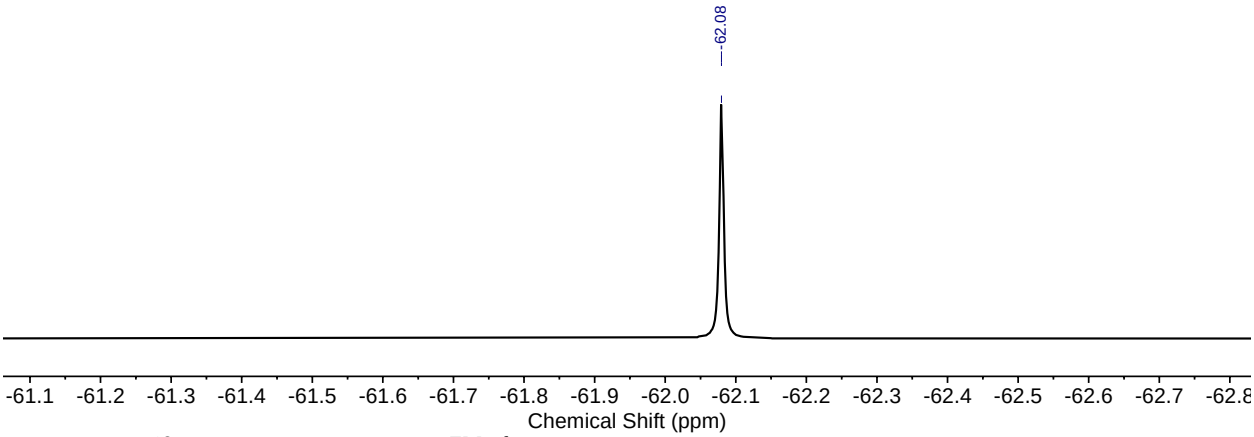

Figure S8. ^{19}F NMR spectrum of (^{EMind}L)Cu(toluene) (**3**), (470 MHz, C_7D_8).

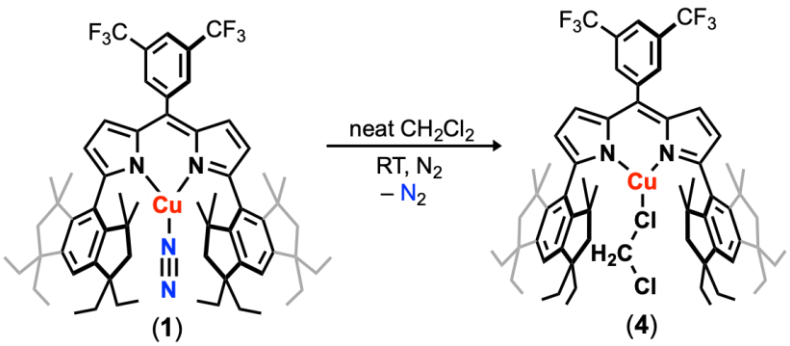

(EMindL)Cu(CH$_2$Cl$_2$) (**4**). In an argon-filled drybox, dissolution of (^{EMind}L)Cu(N$_2$) (**1**)[4] (0.050 g, 0.046 mmol, 1.0 equiv.) into dichloromethane (1 mL) afforded rapid effervescence with a color change to orange-red. The mixture was physically agitated for 30 seconds, followed by removal of solvent *in vacuo* to afford (^{EMind}L)Cu(CH$_2$Cl$_2$) (**5**) in quantitative yield. Single crystals suitable for X-ray diffraction were obtained by reverse vapor diffusion of a dilute 100:1 pentane/dichloromethane solution of **4** into hexamethyldisiloxane at –35 ºC under Ar over 7 days. ^{1}H NMR (500 MHz, CD$_2$Cl$_2$): δ 8.09 (s, 2*H*, fluorinated aryl C–*H*), 8.03 (s, 1*H*, fluorinated aryl C–*H*), 6.75 (br, 2*H*, EMind aryl C–*H*), 6.34 (d, *J* = 4.1 Hz, 2*H*, dipyrrin C–*H*), 6.26 (d, *J* = 4.1 Hz, 2*H*, dipyrrin C–*H*), 5.32 (s, 2*H*, dichloromethane C–*H*), 1.82 (s, 8*H*, EMind aliphatic C–*H*), 1.52 – 1.74 (m, 12*H*, EMind ethyl C–*H*), 1.25 – 1.34 (m, 4*H*, EMind ethyl C–*H*), 1.15 (s, 12*H*, EMind methyl C–*H*), 1.10 (s, 12*H*, EMind methyl C–*H*), 0.78 – 0.91 (24*H*, overlapping triplet EMind ethyl C–*H*). ^{13}C{^{1}H} NMR (100 MHz, C$_6$D$_6$): δ 158.01, 148.44, 148.41, 142.78, 142.71, 138.54, 131.74, 130.98, 130.73, 130.40, 130.07, 129.74, 129.16, 128.33, 127.71, 124.99, 122.90, 122.28, 121.79, 120.10, 119.57, 47.88, 43.67, 34.17, 32.82, 32.76, 32.26, 31.44, 22.38, 13.85, 9.03, 8.82. ^{19}F NMR (470 MHz, C$_6$D$_6$): δ –62.76 (s, fluorinated aryl C*F*$_3$). A satisfactory elemental analysis of **4** could not be obtained due to the instability of the complex in the absence of excess dichloromethane under a N$_2$ atmosphere.

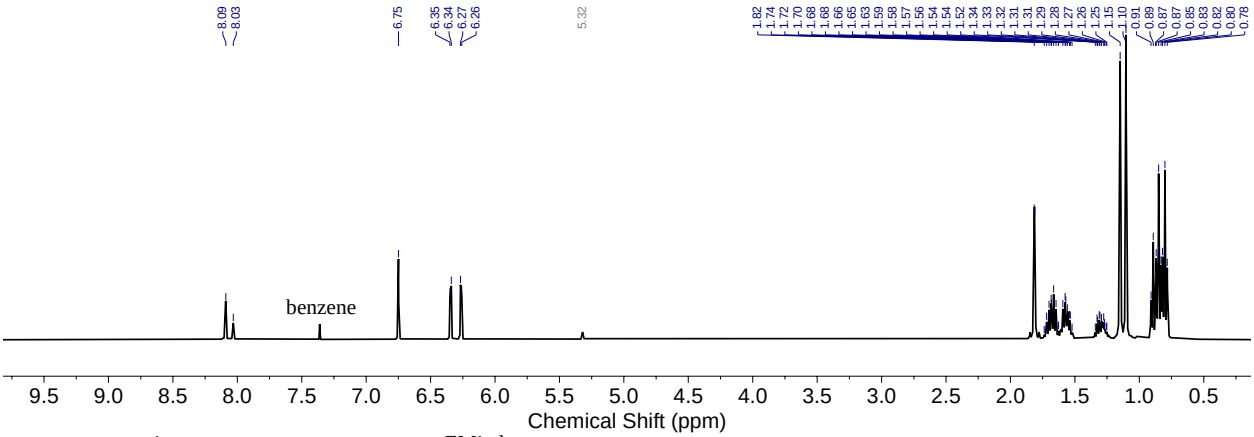

Figure S9. ^{1}H NMR spectrum of ($^{EMind}L$)Cu(CH_2Cl_2) (**4**), (500 MHz, CD_2Cl_2).

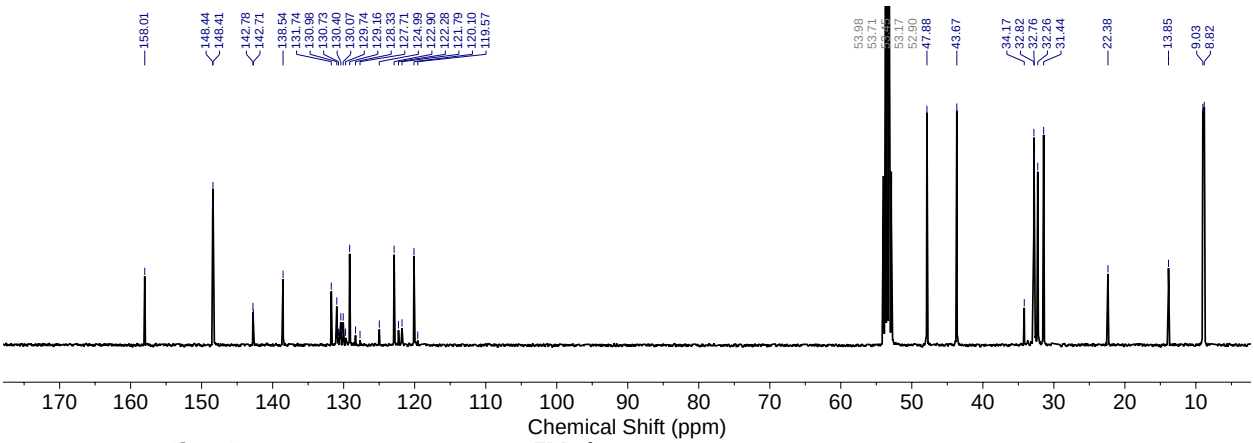

Figure S10. $^{13}C\{^{1}H\}$ NMR spectrum of ($^{EMind}L$)Cu(CH_2Cl_2) (**4**), (125 MHz, CD_2Cl_2).

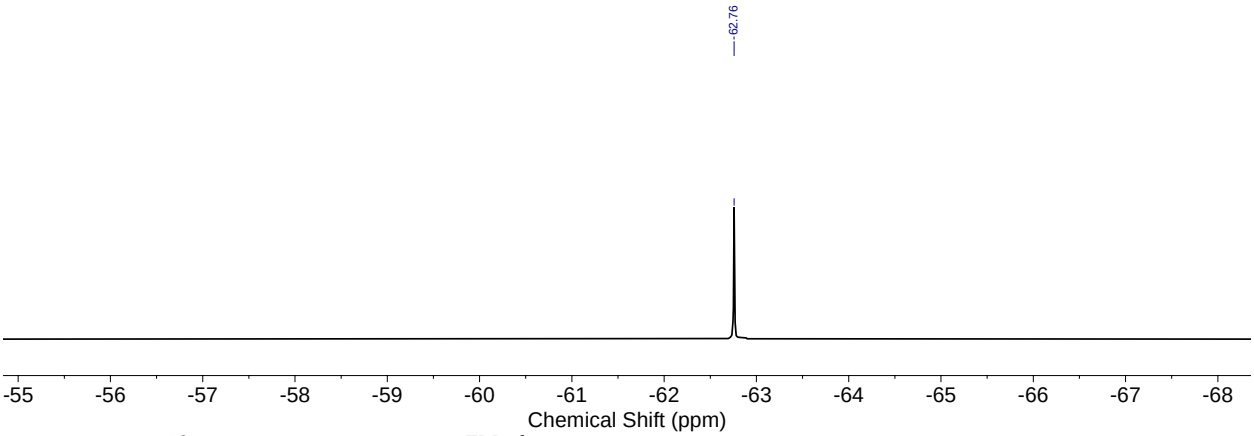

Figure S11. ^{19}F NMR spectrum of ($^{EMind}L$)Cu(CH_2Cl_2) (**4**), (470 MHz, C_6D_6).

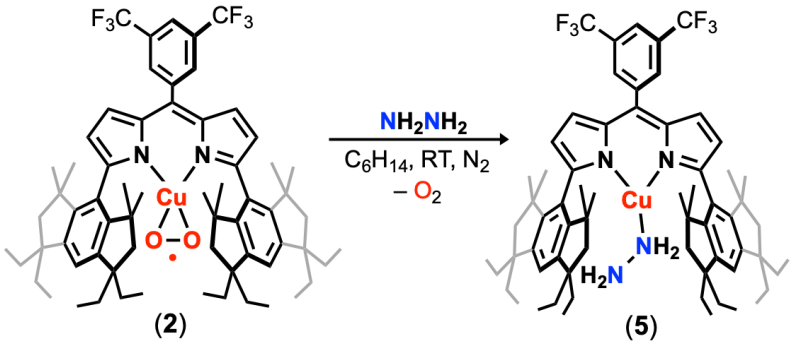

(EMindL)Cu(NH2NH2) (**5**). Under air, to a stirring solution of (EMindL)Cu(O_2) (**2**) (0.050 g, 0.044 mmol, 1.0 equiv.) in hexanes (1 mL) was added excess $NH_2NH_2(H_2O)$ (*ca*. 3.0 equiv.), resulting in rapid effervescence and a color change to bright orange. The mixture was agitated for 30 seconds, followed by removal of solvent *in vacuo* to afford (EMindL)Cu(NH_2NH_2) (**5**) in quantitative yield. Single crystals suitable for X-ray diffraction were obtained by allowing a concentrated pentane solution of **5** to stand at –35 ºC under N_2 for 24 h or at –10 ºC under air for 72 h. ^{1}H NMR (500 MHz, C_6D_6): δ 7.98 (s, 2*H*, fluorinated aryl C–*H*), 7.83 (s, 1*H*, fluorinated aryl C–*H*), 6.73 (s, 2*H*, EMind aryl C–*H*), 6.58 (d, *J* = 4.3 Hz, 2*H*, dipyrrin C–*H*), 6.42 (d, *J* = 4.4 Hz, 2*H*, dipyrrin C–*H*), 2.45 (s, 4*H*, hydrazine N–*H*), 1.71 – 1.79 (8*H*, overlapping singlet EMind aliphatic C–*H*), 1.50 – 1.68 (16*H*, overlapping multiplet from EMind ethyl C–*H*), 1.43 (s, 12*H*, EMind methyl C–*H*), 1.35 (s, 12*H*, EMind methyl C–*H*), 0.82 (t, *J* = 7.3 Hz, 12*H*, EMind ethyl C–*H*), 0.76 (t, *J* = 7.3 Hz, 12*H*, EMind ethyl C–*H*). ^{13}C{^{1}H} NMR (100 MHz, C_6D_6): δ 157.19, 149.06, 148.06, 143.26, 142.88, 138.66, 133.71, 131.01, 130.57, 130.24, 129.02, 124.91, 122.27, 122.20, 121.45, 119.17, 52.52, 48.06, 43.88, 34.12, 32.95, 32.80, 31.89, 22.40, 13.95, 9.03. ^{19}F NMR (470 MHz, C_6D_6): –62.91 (s, fluorinated aryl CF_3). Anal. Calc. for $C_{65}H_{85}CuF_6N_4$•C_5H_{12}: C 71.73, H 8.34, N 4.78; Found: C 72.20, H 8.28, N 5.10 (one molecule of pentane is present from bulk recrystallization and is located in the unit cell).

Note: The preparation of (EMindL)Cu(NH_2NH_2) (**5**) is similarly accomplished by treatment of (EMindL)Cu(N_2) (**1**)[4] with excess anhydrous hydrazine in hexanes, followed by removal of solvent to afford **6** in quantitative yield.

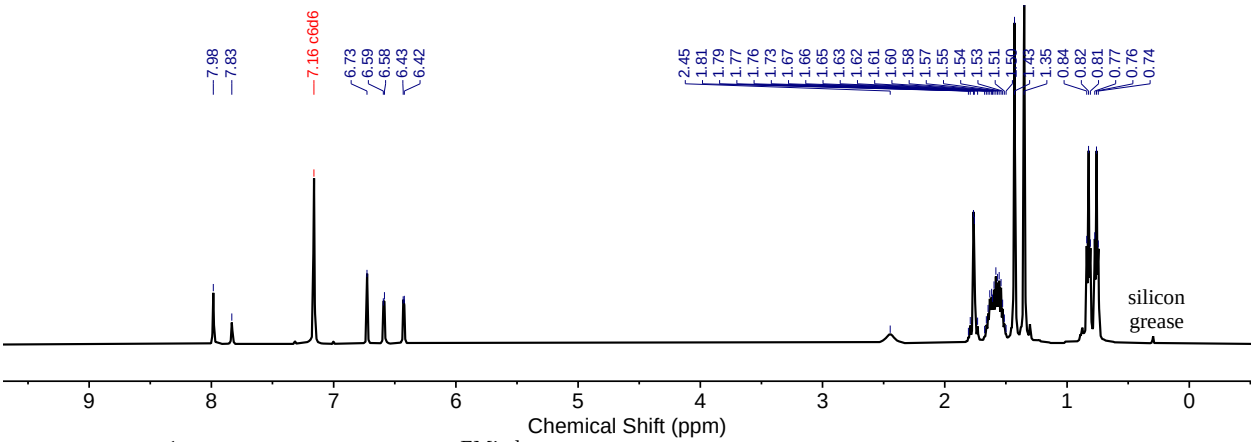

Figure S12. ^{1}H NMR spectrum of (^{EMind}L)Cu(NH_2NH_2) (**5**), (500 MHz, C_6D_6).

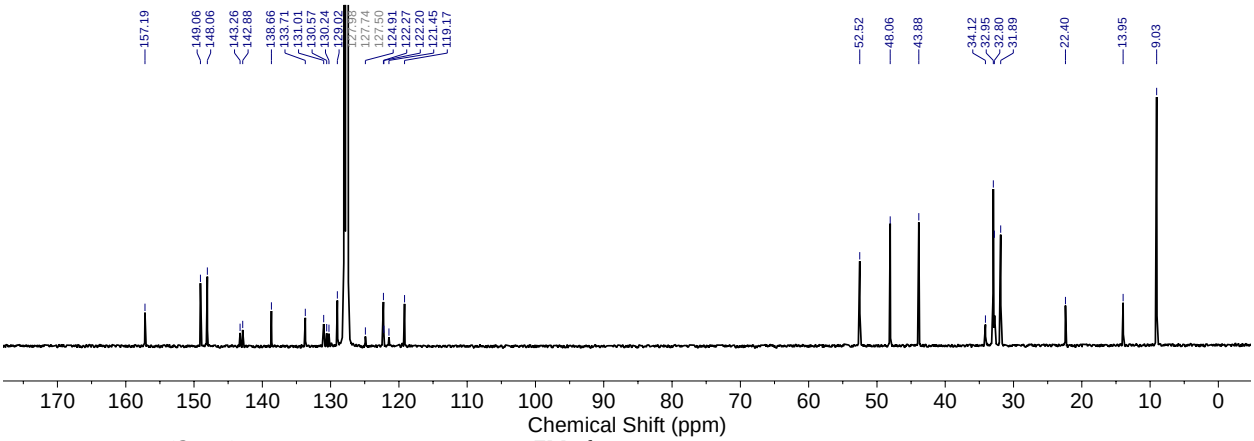

Figure S13. ^{13}C{^{1}H} NMR spectrum of (^{EMind}L)Cu(NH_2NH_2) (**5**), (100 MHz, C_6D_6).

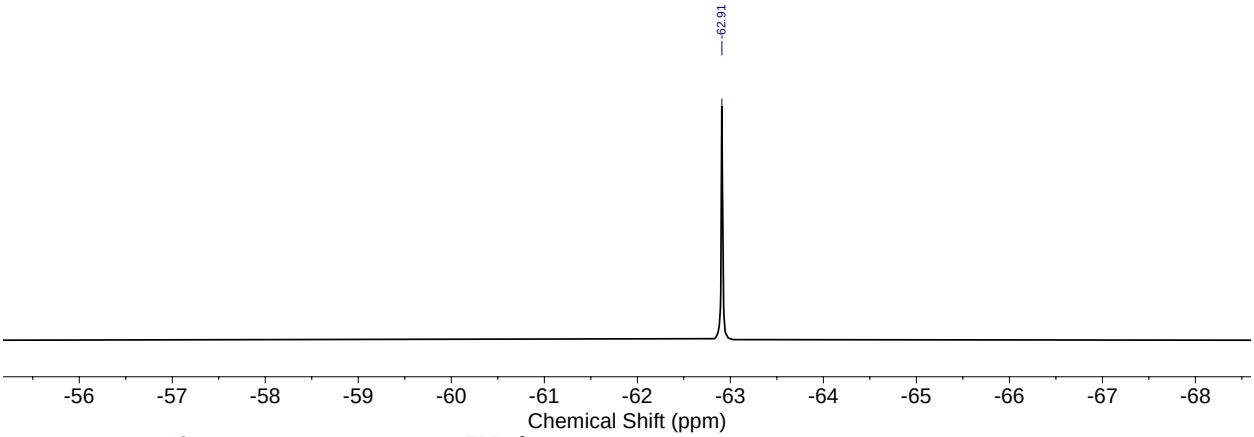

Figure S14. ^{19}F NMR spectrum of (^{EMind}L)Cu(NH_2NH_2) (**5**), (470 MHz, C_6D_6).

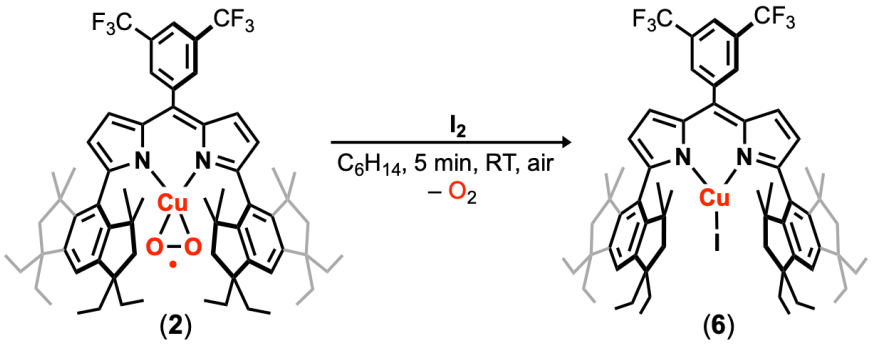

(^{EMind}L)CuI (**6**). Under ambient air, elemental iodine (0.028 g, 0.110 mmol, 1.0 equiv.) was added as a solid to a solution of **2** (0.120 g, 0.110 mmol, 1.0 equiv.) in hexanes (2 mL), resulting in immediate effervescence and a darkening of the solution to dark pink. The solution was stirred for five minutes, followed by removal of solvent *in vacuo*. Removal of excess elemental iodine could be conducted either through (i) prolonged heating (60 ºC, 24 h) under dynamic vacuum or through (ii) lyophilization, followed by suspending the residual solid in cold acetonitrile (*ca*. 1 mL), rinsing over Celite, and eluting with warm benzene to afford (^{EMind}L)CuI (**6**) as a brown-pink solid in essentially quantitively yield. Single crystals suitable for X-ray diffraction were obtained by allowing layering a concentrated pentane solution of **6** to stand at –35 ºC for 72 h. ^{1}H NMR (500 MHz, C_6D_6): δ 8.41 (v. br), 8.16 (br), 3.25 (v. br), 2.63 (br), 1.79 (v. br), 1.05 (v. br), 0.69 (v. br), 0.43 (br). ^{19}F NMR (470 MHz, C_6D_6): –62.11. UV/vis (C_6H_{14}) λ_{max}/cm^{-1} (ε/M^{-1} cm^{-1}): 700 (2,200) 525 (62,000), 500 (20,200), 380 (3,900), 310 (8,200). Anal. Calc. for $C_{65}H_{81}CuF_6IN_2$•CH_3CN: C 65.11, H 6.85, N 3.40; Found: C 65.43, H 6.58, N 3.71.

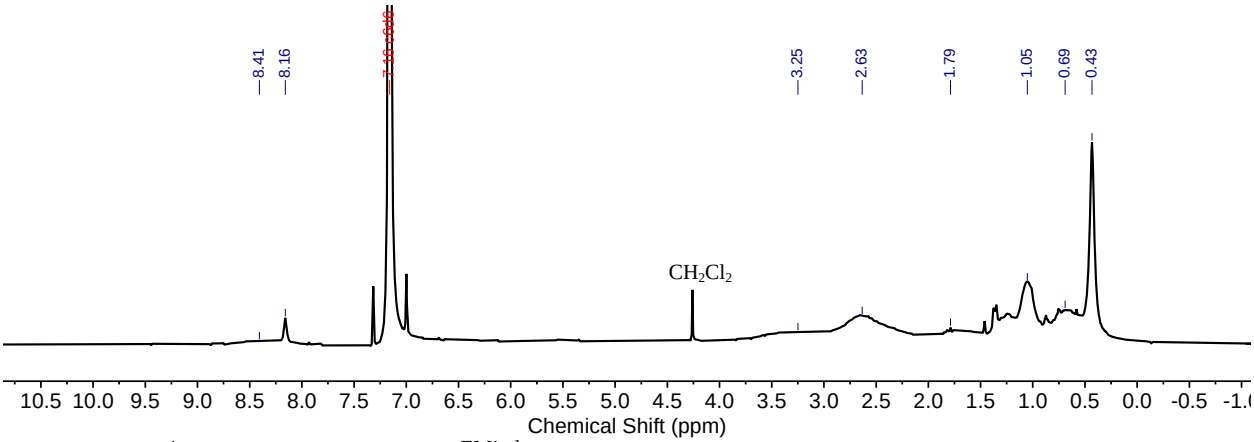

Figure S15. ^{1}H NMR spectrum of (^{EMind}L)CuI (**6**), (500 MHz, C_6D_6).

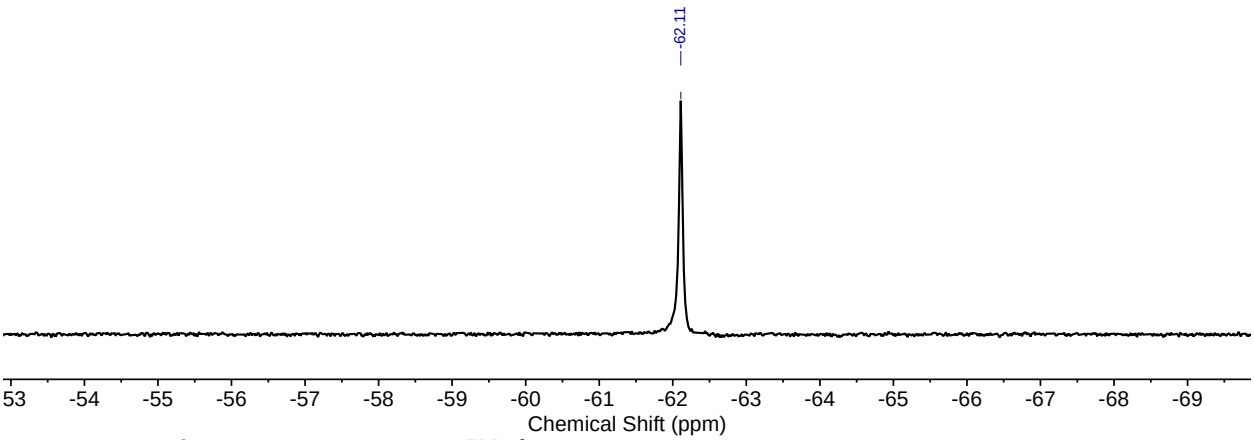

Figure S16. ^{19}F NMR spectrum of (^{EMind}L)CuI (**6**), (470 MHz, C_6D_6).

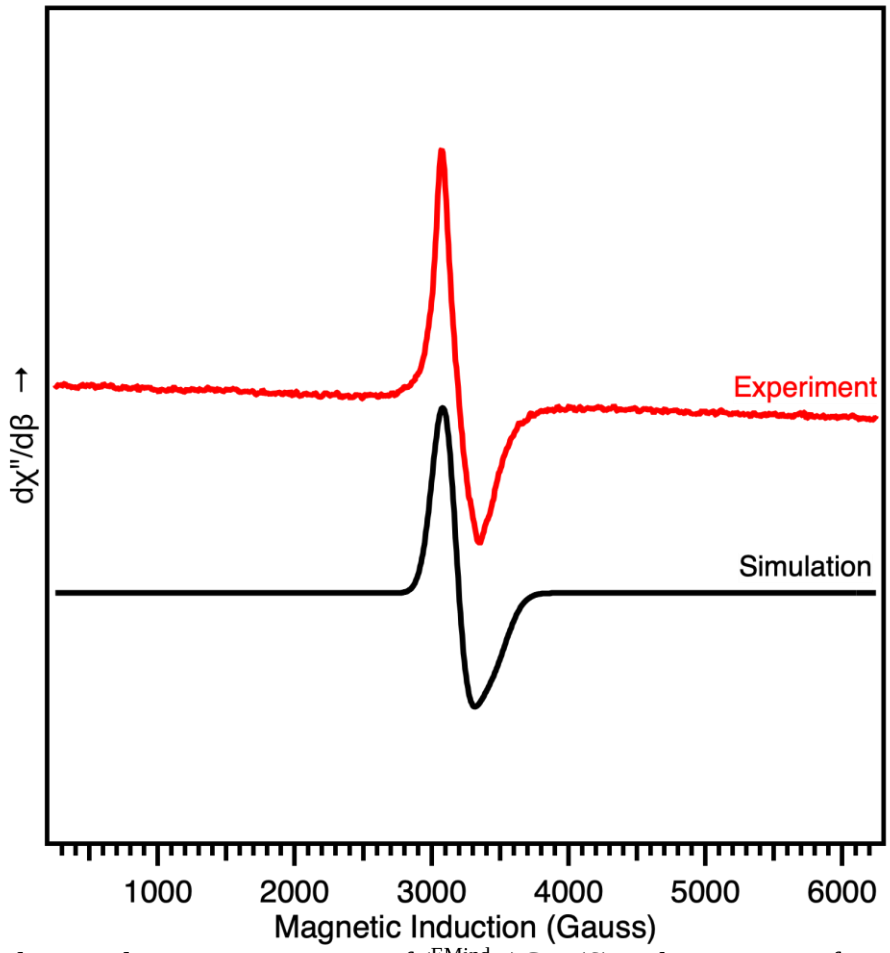

Figure S17. Solution toluene EPR spectrum of (^{EMind}L)CuI (**6**) with microwave frequency of 9.857 GHz and 0.6325 mW microwave power, expanded to show an isotropic S = 1/2 signal (red) simulated using Easyspin (black) with the following parameters: $g_1 = 2.24$, $\sigma g_1 = 0.16$; $g_2 = 2.04$, $\sigma g_2 = 0.17$.

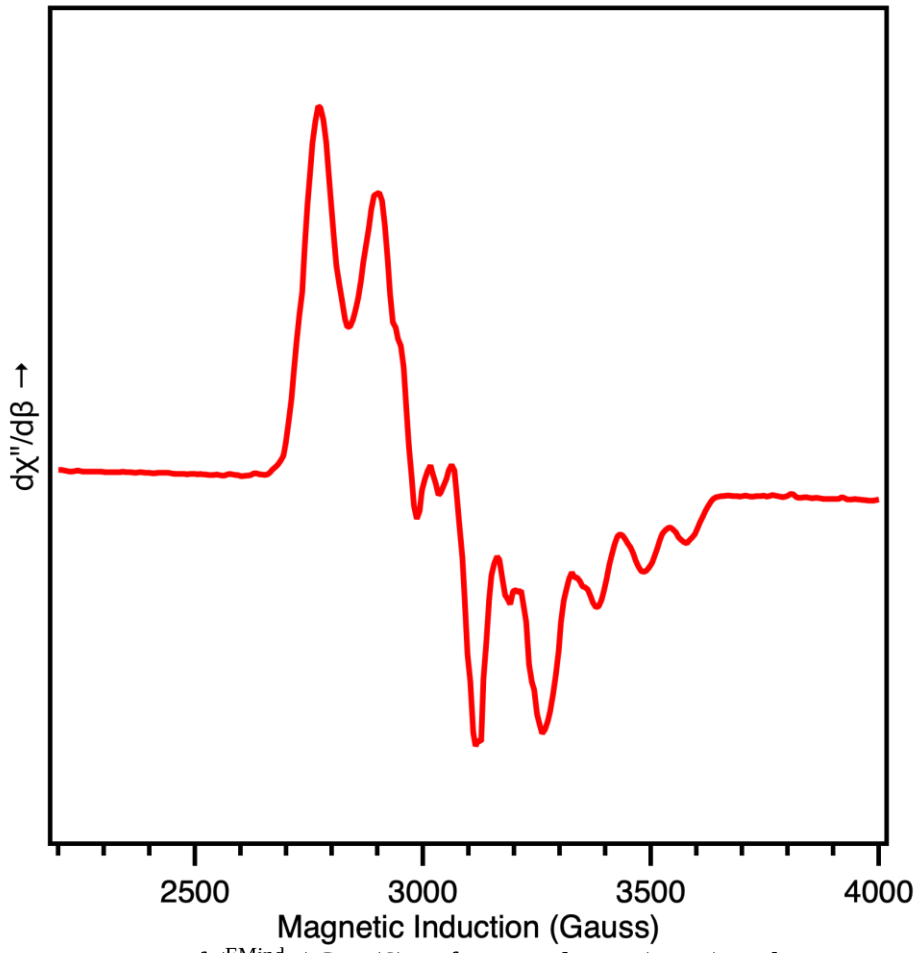

Figure S18. EPR spectrum of (^{EMind}L)CuI (**6**) in frozen toluene (77 K) with microwave frequency of 9.332 GHz and 0.6325 mW microwave power. The anisotropy is attributed to the heavy-iodine atom.

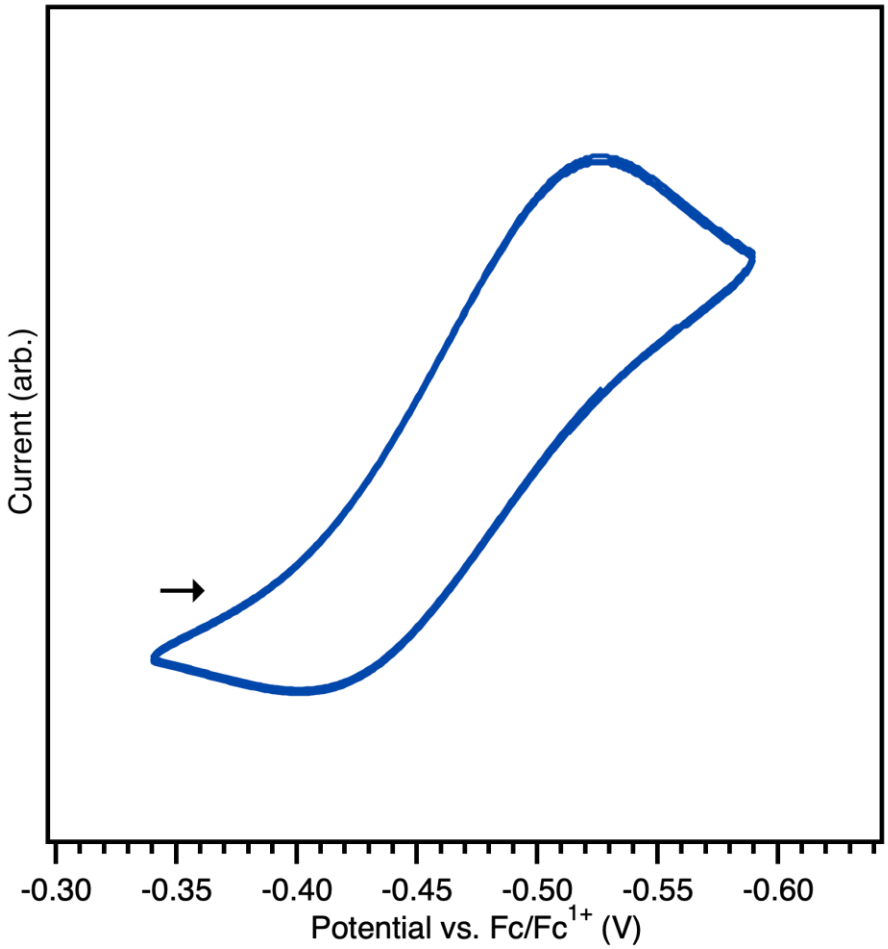

Figure S19. Quasi-reversible one-electron reduction of (^{EMind}L)CuI (**6**), ($E_{1/2}$ = –0.46 V vs. Fc/Fc^{1+}) at a scan rate of 100 mV s^{-1}. The data was recorded in 1,2-difluorobenzene at a concentration of ca. 0.01 mM, with glassy carbon, Pt-wire, and Ag-wire as the working, counter, and reference electrodes, respectively. Arrows denote initial scan direction. Saturated tetrabutylammonium hexafluorophosphate ($[^{n}Bu_4N][PF_6]$) solutions of 0.2 M in 1,2-difluorobenzene were prepared before each experiment in the presence of molecular sieves to remove trace water. No background reaction between **8** and the electrolyte was observed.

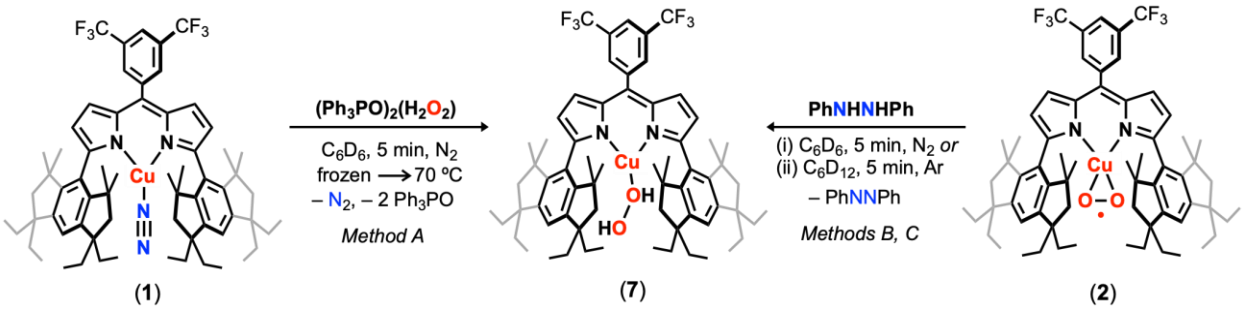

(^{EMind}L)Cu(H_2O_2) (**7**). The *in situ* preparation of (^{EMind}L)Cu(H_2O_2) (**7**) could be achieved in three separate protocols:

Method A. In a dinitrogen-filled drybox, crystalline (^{EMind}L)Cu(N_2) (**1**)[4] (0.008 g, 0.007 mmol, 1.0 equiv.) was dissolved in C_6D_6 (*ca*. 0.4 mL), resulting in effervescence and a subtle color change to red-orange, indicative of (^{EMind}L)Cu(C_6D_6). The mixture was transferred to an NMR tube and frozen in a liquid-nitrogen chilled cold well. Upon thawing, $(Ph_3PO)_2(H_2O_2)$[2] (0.005 g, 0.008 mmol, 1.1 equiv.) was added in C_6D_6 (*ca*. 0.3 mL), resulting in a slight darkening of the solution. Analysis by multinuclear NMR spectroscopy revealed full consumption of (^{EMind}L)Cu(C_6D_6), accompanied by formation of triphenylphosphine oxide and formation of a new Cu-containing product, assigned as (^{EMind}L)Cu(H_2O_2) (**7**). ^{1}H NMR (500 MHz, C_6D_6): δ 7.91 (s, 1*H*, fluorinated aryl C–*H*), 7.85 (s, 1*H*, fluorinated aryl C–*H*), 7.04 (broad s, 2*H*, EMind aryl C–*H*), 6.48 (d, *J* = 4.2 Hz, 2*H*, dipyrrin C–*H*), 6.25 (d, *J* = 4.2 Hz, 1*H*, dipyrrin C–*H*), 1.56 – 1.91 (24*H*, overlapping singlet 8*H* from EMind aliphatic C–*H* and multiplet 16*H* from EMind ethyl C–*H*), 1.30 (s, 24*H*, EMind methyl C–*H*), 0.89 (apparent quintet from overlapping triplets, *J* = 7.4 Hz, 24*H*, EMind ethyl C–*H*). ^{19}F NMR (470 MHz, C_6D_6): δ –62.36 (s, fluorinated aryl CF_3). Partial removal of triphenylphosphine could be achieved by filtering a just-thawed solution of **7** in minimal pentane. Control experiments reveal no background changes by NMR spectroscopy of (^{EMind}L)Cu(N_2) upon addition of excess triphenylphosphine. Formation of (^{EMind}L)Cu(H_2O) was achieved through treatment of (^{EMind}L)Cu(N_2) with stoichiometric water, which exhibited distinct ^{1}H/^{19}F NMR resonances from **7** (*manuscript in preparation*).

Method B. In a dinitrogen-filled drybox, to a thawing solution of (^{EMind}L)Cu(O_2) (**2**) in C_6D_6 (containing *ca*. 5 % (^{EMind}L)Cu(N_2) due to solution equilibration) was added stoichiometric 1,2-diphenylhydrazine. Analysis by multinuclear (^{1}H/^{19}F) NMR spectroscopy reveals consumption of (^{EMind}L)Cu(O_2) (**2**) and formation of both (^{EMind}L)Cu(N_2) (**1**), azoarene, and a new Cu-containing product identical to that obtained from *Method A*. Control experiments reveal no background reaction of (^{EMind}L)Cu(O_2) with either 1,2-diphenylhydrazine or the corresponding azoarene.

Method C. In an argon-filled drybox, to a solution of (^{EMind}L)Cu(O_2) (**2**) in C_6D_{12} was added stoichiometric 1,2-diphenylhydrazine. Analysis by multinuclear (^{1}H/^{19}F) NMR spectroscopy reveals consumption of (^{EMind}L)Cu(O_2) (**2**) and formation of a new diamagnetic species, identical to the product from *Method A*. Control experiments reveal no background reaction of (^{EMind}L)Cu(O_2) (**2**) with either 1,2-diphenylhydrazine or the corresponding azoarene.

Note I – The aliphatic resonance attributed to the EMind methyl C–H is a single resonance (24*H* integration) in (^{EMind}L)Cu(H_2O_2) (**7**), contrasting the two singlet resonances in (^{EMind}L)Cu(C_6D_6) for the same EMind methyl C–H (2 x 12*H* integration). This chemical difference indicates that **7** is a distinct diamagnetic species compared to **1**.

Note II – Allowing solutions of (^{EMind}L)Cu(H_2O_2) (**7**) to stand in C_6D_6 over hours affords increasing amounts of (^{EMind}L)H, attributed to the acidicity of H_2O_2 resulting in proteo-demetallation. Attempts at crystallizing **7** under N_2 as concentrated solutions of neat pentane has resulted in formation of crystalline **1**.

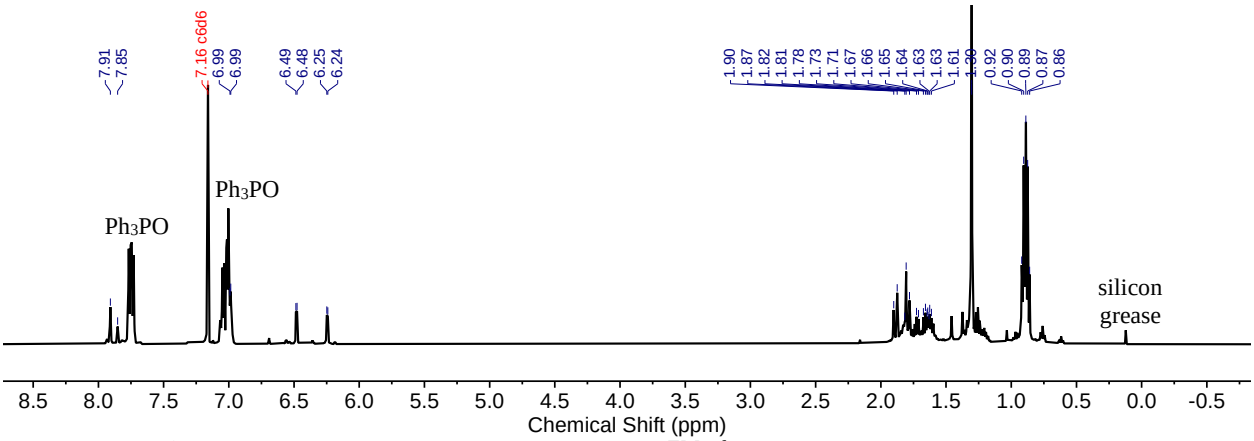

Figure S20. ^{1}H NMR spectrum of *in situ* prepared (^{EMind}L)Cu(H_2O_2) (**7**), (500 MHz, C_6D_6).

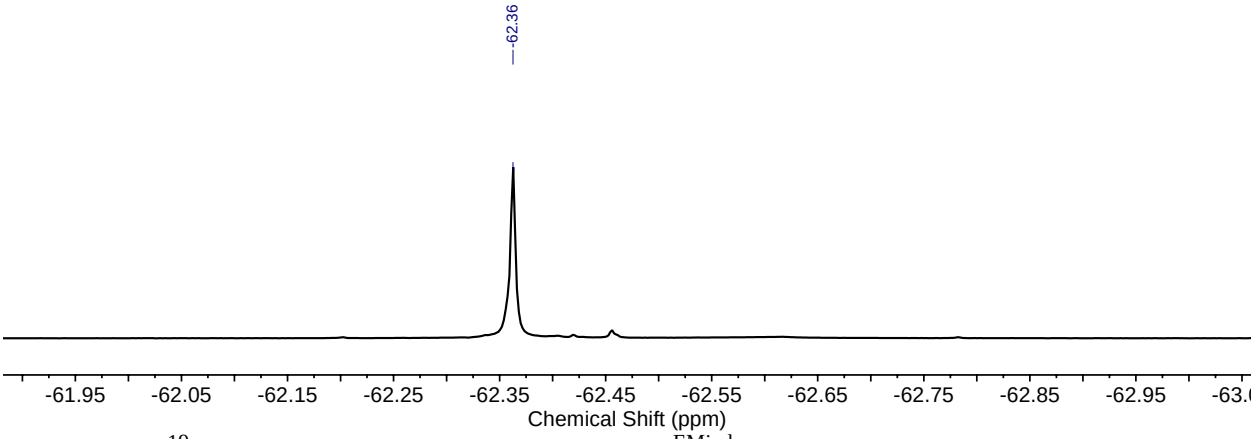

Figure S21. ^{19}F NMR spectrum of *in situ* prepared (^{EMind}L)Cu(H_2O_2) (**7**), (470 MHz, C_6D_6).

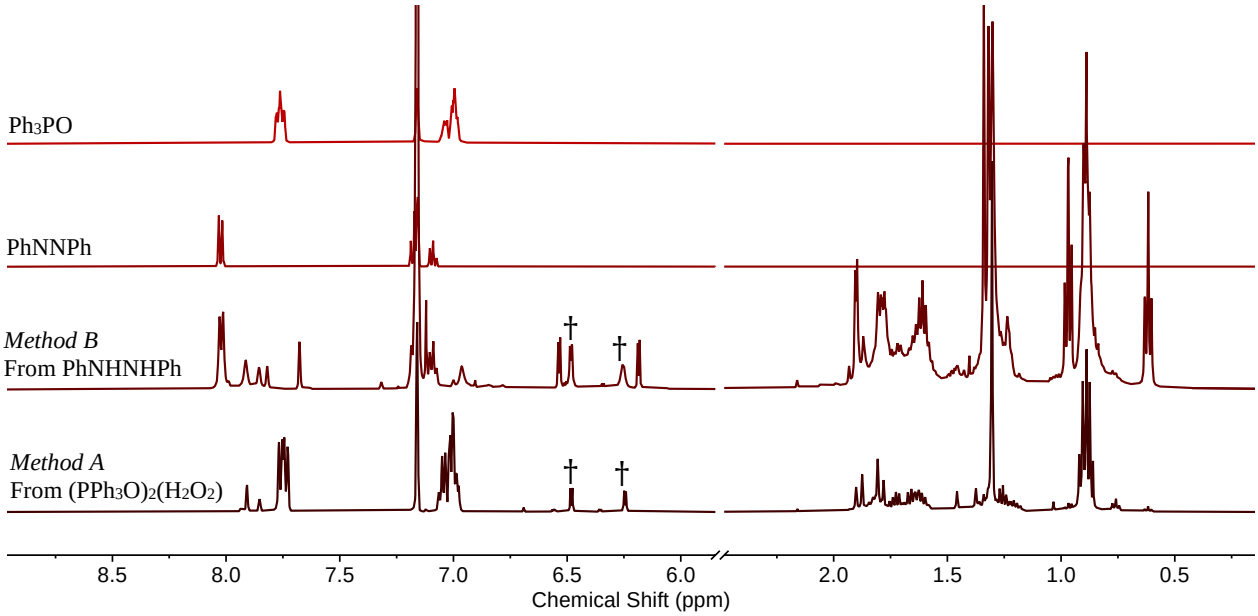

Figure S22. ^{1}H NMR spectra overlay (500 MHz, C_6D_6) of (^{EMind}L)Cu(H_2O_2) (**7**) prepared by ($PPh_3O)_2(H_2O_2$) (*bottom*) and by treatment of (^{EMind}L)Cu(O_2) (**2**) with PhNHNHPh (*lower middle*, unassigned resonances correspond to unreacted **2**). Reference azoarene (*upper middle*) and PPh_3O (*top*) are presented as ^{1}H NMR comparison spectra. Obelisk refers to diagnostic dipyrrin C–*H* resonances.

Supporting Spectroscopic Characterization.

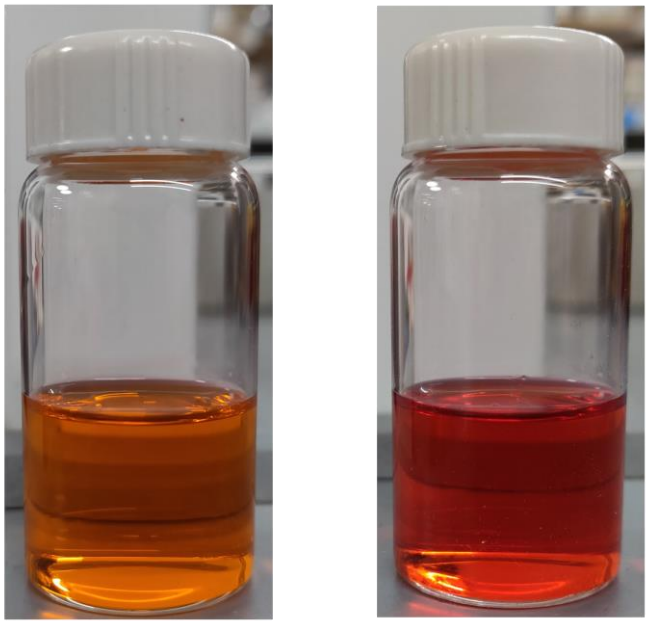

Figure S23. Visual comparison of (^{EMind}L)Cu(N_2) (**1**) in hexanes at 20 μM concentration (*left*, *orange*) and subsequent air exposure and agitation over five seconds to yield (^{EMind}L)Cu(O_2) (**2**) in quantitative yield.

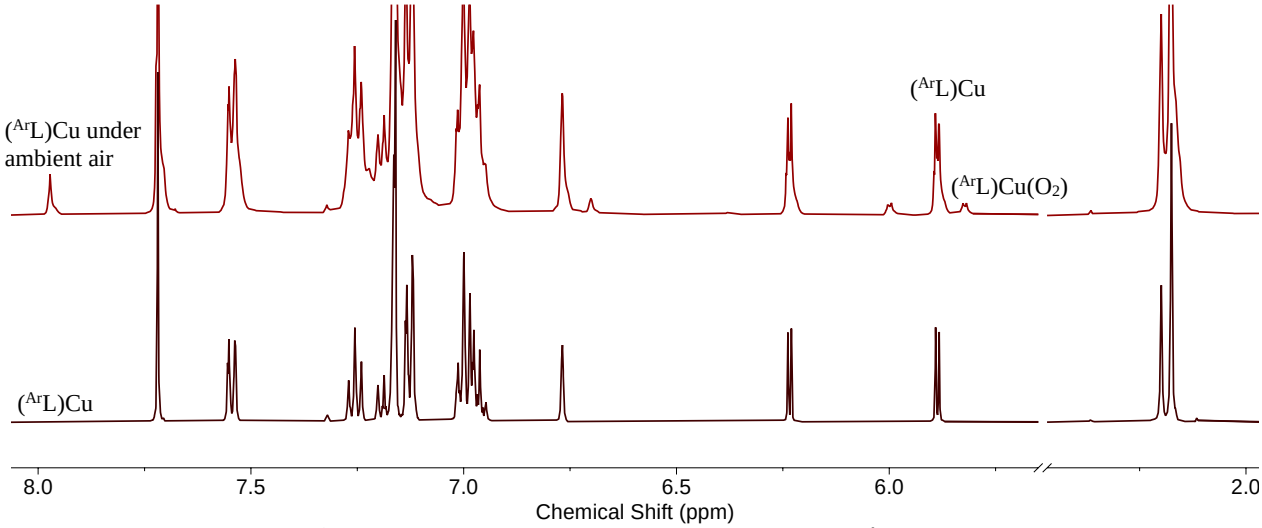

Figure S24. Truncated ^{1}H NMR spectra of (500 MHz, C_6D_6) of (^{Ar}L)Cu (*bottom*, *maroon*) with subsequent air exposure, yielding growth of (^{Ar}L)Cu(O_2) within five minutes prior to formation of additional paramagnetic species and (^{Ar}L)H (*top*, *red*).

O_2 Transfer from (^{EMind}L)Cu(O_2) (2) to $IMes_2Pd$.

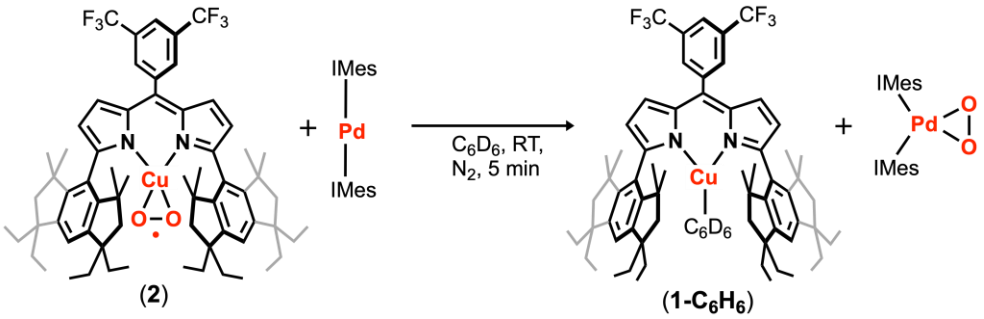

General Procedures. In a dinitrogen-filled drybox, a yellow solution[3] of $IMes_2Pd$ (0.005 g, 0.007 mmol, 1.0 equiv.) in C_6D_6 (*ca.* 0.5 mL) was added to solid (^{EMind}L)Cu(O_2) (**2**) (0.006 g, 0.007 mmol, 1.0 equiv.), resulting in a Carmine red solution which changed color to orange within five minutes. The solution was then transferred to an NMR tube and checked by multinuclear (^{1}H/^{19}F) NMR spectroscopy (500 MHz), revealing formation of $IMes_2Pd(O_2)$ and (^{EMind}L)Cu(η^2-C_6D_6) (**1-benzene**) as the major species. Analysis by ^{19}F NMR reveals *ca*. 80 % of ^{19}F active species as **1-benzene.**

Note – **2** should be imported into the drybox immediately prior to the reaction, noting prolonged exposure of **2** to a dinitrogen atmosphere affords trace quantities of O_2 dissociation.

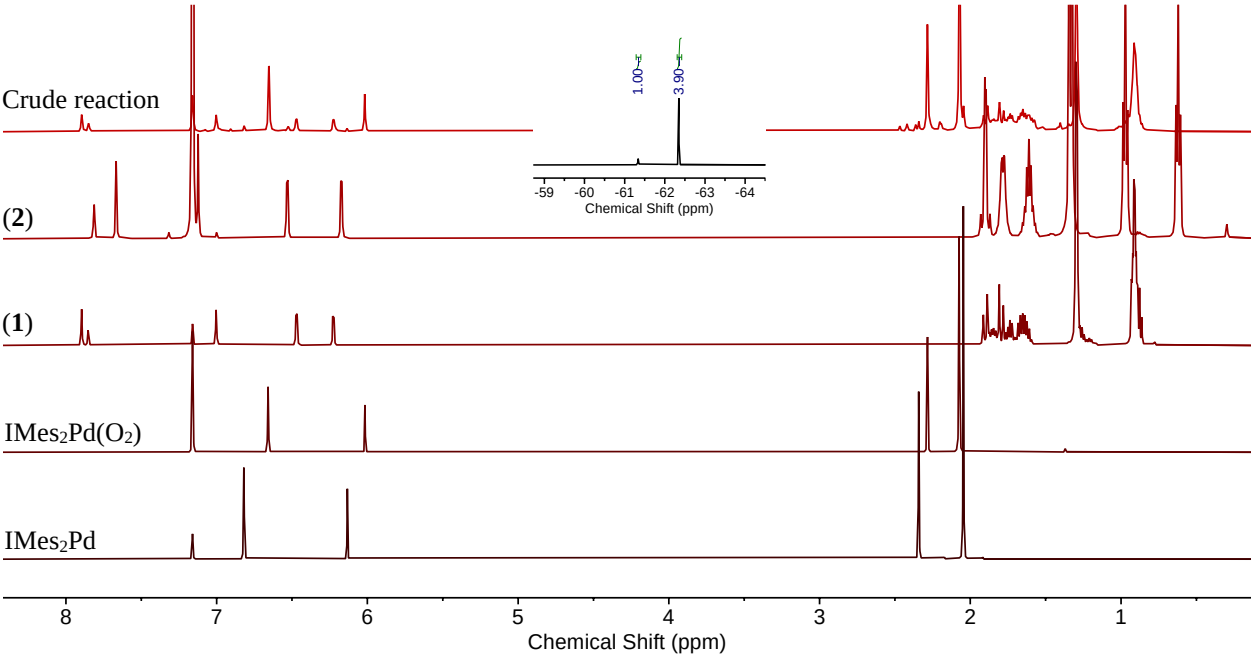

Figure S25. Stacked ^{1}H NMR spectra (500 MHz, C_6D_6) of $IMes_2Pd$ (*bottom*), $IMes_2Pd(O_2)$ (*lower bottom*), (^{EMind}L)Cu(η^2-C_6D_6) (**1-benzene**) (*middle*), (^{EMind}L)Cu(O_2) (**2**) (*upper top*), and crude reaction mixture (*top*). A trace quantity of $IMes_2Pd$ is observed in the crude reaction mixture, attributed to release of O_2 from **2** under N_2. Inset reveals approximately 80 % of the ^{19}F NMR active resonances are attributed to formation of **1**.

O_2 Displacement through Solvent Exchange.

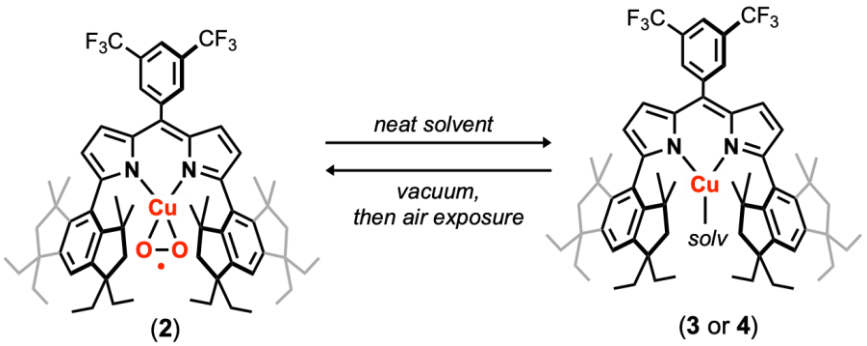

(**2**) (**3** or **4**)

General procedure. Under air, (^{EMind}L)Cu(O_2) (**2**) (*ca.* 0.010 g, 0.010 mmol) was dissolved in the specified solvent (*ca*. 0.5 mL) and agitated until effervescence ceased. The solution was then transferred to an NMR tube and checked by multinuclear (^{1}H/^{19}F) NMR spectroscopy (500 MHz). Titration experiments of the specified solvent establish the identity of the new species as the solvent adduct with the secondary species as **2**, as the ratio of the new species to **2** was correlated with increasing equivalents of solvents. The contents of the NMR tube were subsequently transferred to a scintillation vial with removal of solvent *in vacuo* by rotary evaporation. The contents were subsequently dissolved in C_6D_6 and analyzed by multinuclear (^{1}H/^{19}F) NMR spectroscopy (500 MHz). Assignments were supported by comparison to authentic samples of **2**.

Note – all solvents, including C_6D_6, were checked by ^{1}H NMR to ensure complete exclusion of CH_2Cl_2 as a possible contaminant, noting facile partial formation of (^{EMind}L)Cu(CH_2Cl_2) (**4**) in the presence of trace dichloromethane. To avoid possible contamination, the storage container of C_6D_6 was only employed in a fume hood strictly devoid of any CH_2Cl_2.

Formation of (^{EMind}L)Cu(toluene) (3) from (^{EMind}L)Cu(O_2) (2).

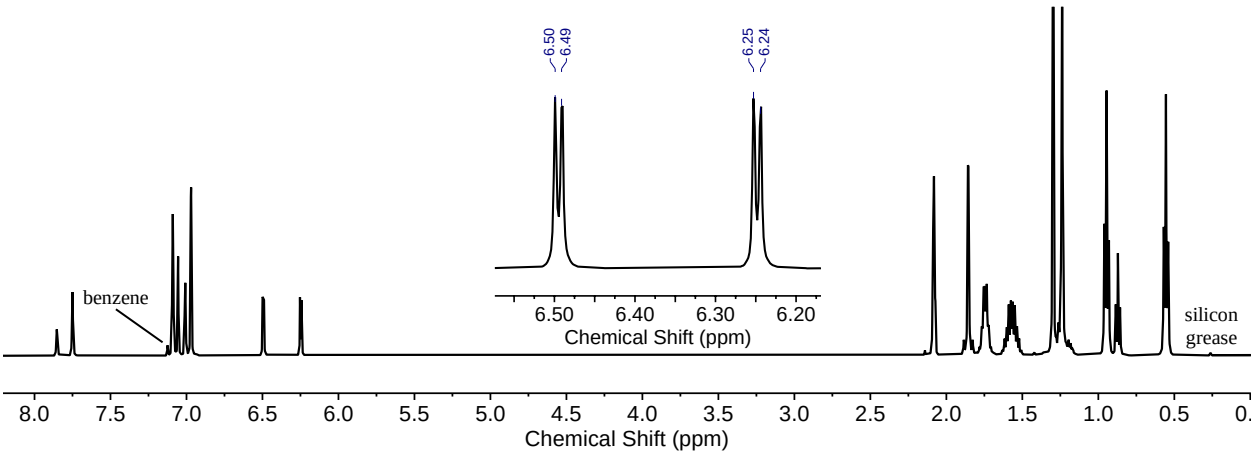

Figure S26. Crude ^{1}H NMR spectrum (500 MHz, C_7D_8) of (^{EMind}L)Cu(toluene) (**3**) prepared by dissolution of (^{EMind}L)Cu(O_2) (**2**) in neat C_7D_8, depicting formation of a single species. Inset highlights the formation of a single dipyrrin-containing based on the sole set of dipyrrin C–*H* resonances.

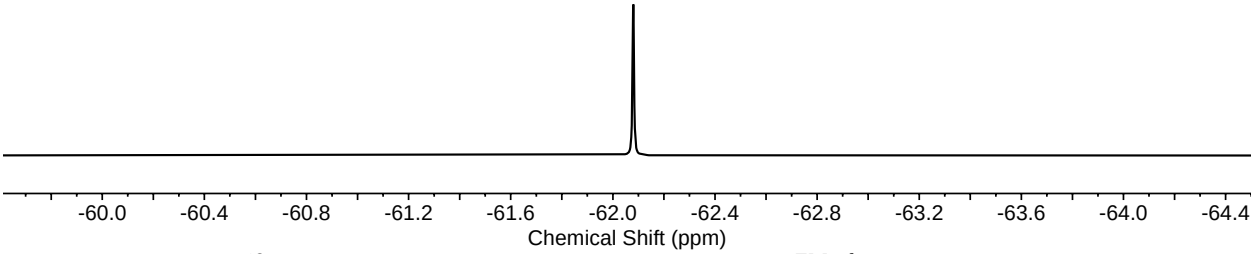

Figure 27. Crude ^{19}F NMR spectrum (500 MHz, C_7D_8) of (^{EMind}L)Cu(toluene) (**3**) prepared by dissolution of (^{EMind}L)Cu(O_2) (**2**) in neat C_7D_8, depicting formation of a single species.

Reformation of (^{EMind}L)Cu(O_2) (2) from (^{EMind}L)Cu(toluene) (3).

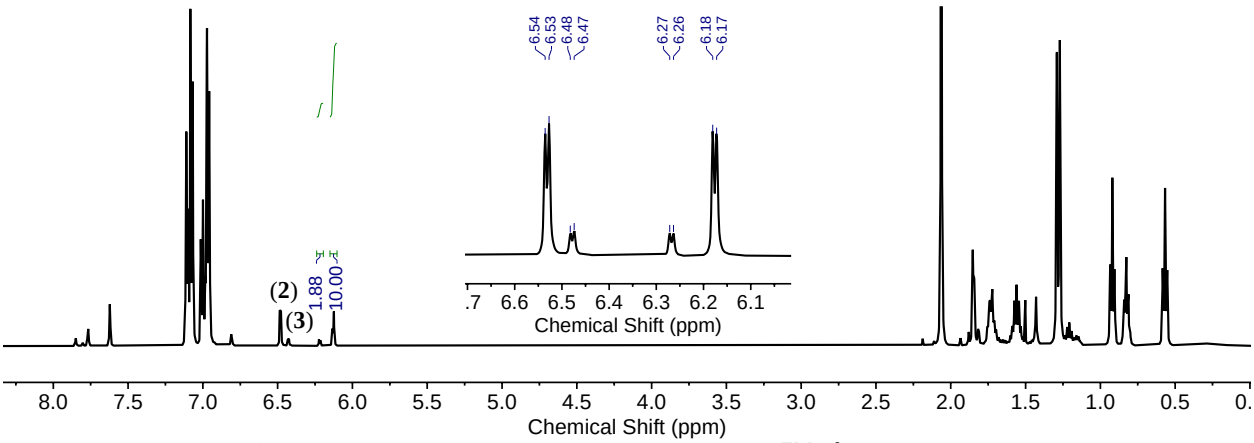

Figure S28. Crude ^{1}H NMR spectrum (500 MHz, C_6D_6) of (^{EMind}L)Cu(O_2) (**2**) prepared under air by removal of solvent from *in situ* prepared (^{EMind}L)Cu(toluene) (**3**). The baseline resonances denote unconverted **3** (*ca*. 16 % by integration). Inset highlights two sets of dipyrrin C–*H* resonances.

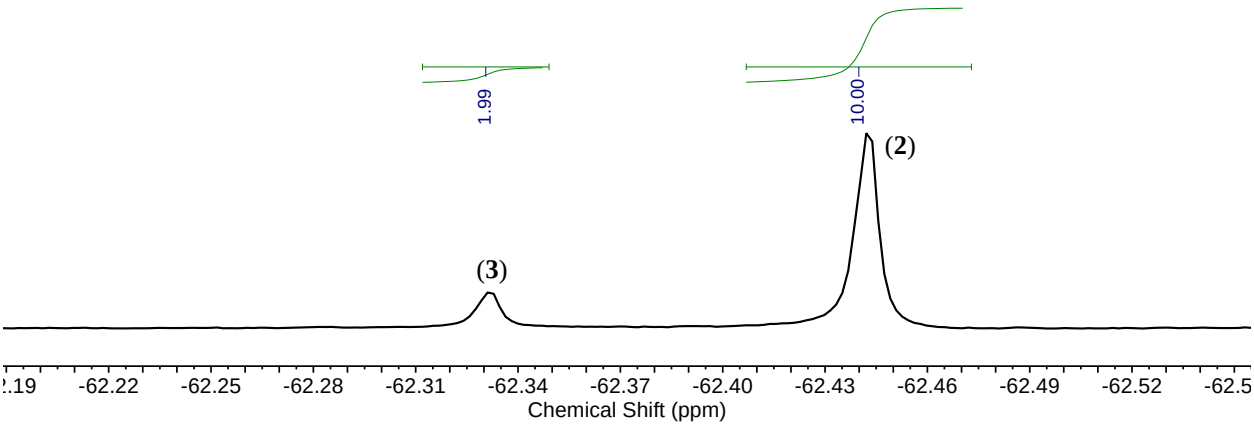

Figure S29. Crude ^{19}F NMR spectrum (470 MHz, C_6D_6) of (^{EMind}L)Cu(O_2) (**2**) prepared under air by removal of solvent from *in situ* prepared (^{EMind}L)Cu(toluene) (**3**). The baseline resonances denote unconverted **3** (*ca*. 16 % by integration).

Formation of (^{EMind}L)Cu(CH_2Cl_2) (4) from (^{EMind}L)Cu(O_2) (2).

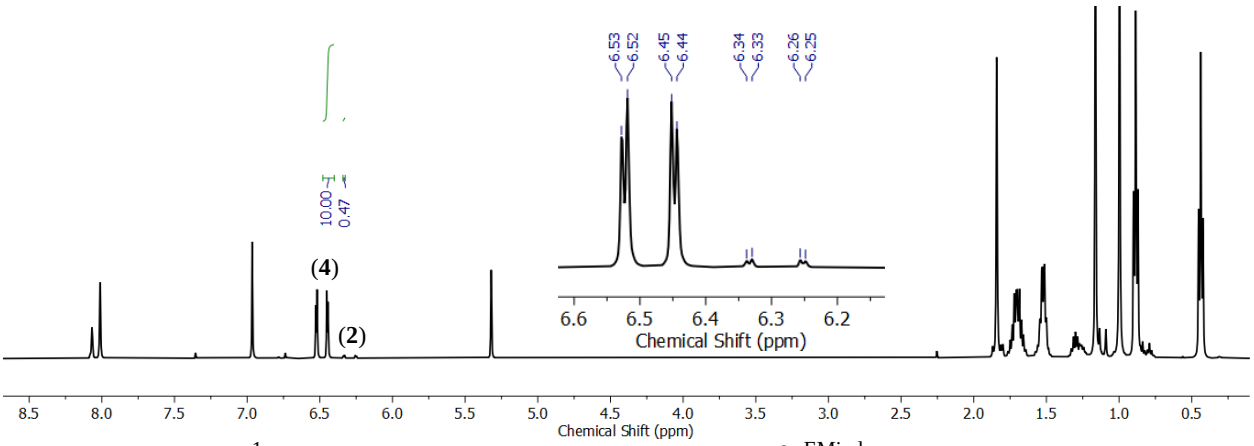

Figure S30. Crude ^{1}H NMR spectrum (500 MHz, CD_2Cl_2) of (^{EMind}L)Cu(CH_2Cl_2) (**4**) prepared by dissolution of (^{EMind}L)Cu(O_2) (**2**) in neat CD_2Cl_2. The baseline resonances denote unconverted **2** (*ca*. 5 % by integration). Inset highlights two sets of dipyrrin C–*H* resonances.

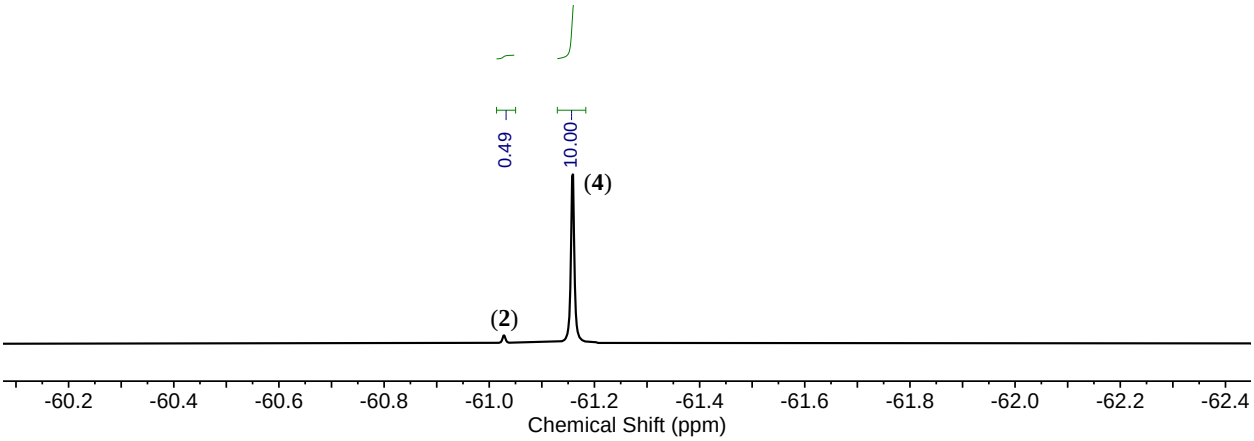

Figure S31. Crude ^{19}F NMR spectrum (470 MHz, CD_2Cl_2) of (^{EMind}L)Cu(CH_2Cl_2) (**4**) prepared by dissolution of (^{EMind}L)Cu(O_2) (**2**) in neat CD_2Cl_2. The baseline resonances denote unconverted **2** (*ca*. 5 % by integration).

Reformation of (^{EMind}L)Cu(O_2) (2) from (^{EMind}L)Cu(CH_2Cl_2) (4).

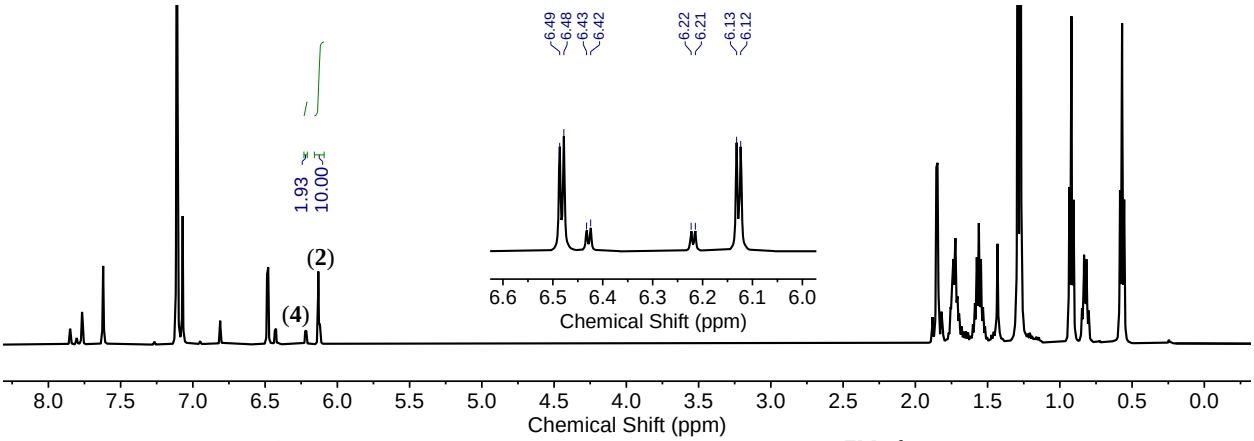

Figure S32. Crude ^{1}H NMR spectrum (500 MHz, C_6D_6) of (^{EMind}L)Cu(O_2) (**2**) prepared by removal of solvent from *in situ* prepared (^{EMind}L)Cu(CH_2Cl_2) (**4**) under air. The baseline resonances denote unconverted **4** (*ca*. 16 % by integration). Inset highlights two sets of dipyrrin C–*H* resonances.

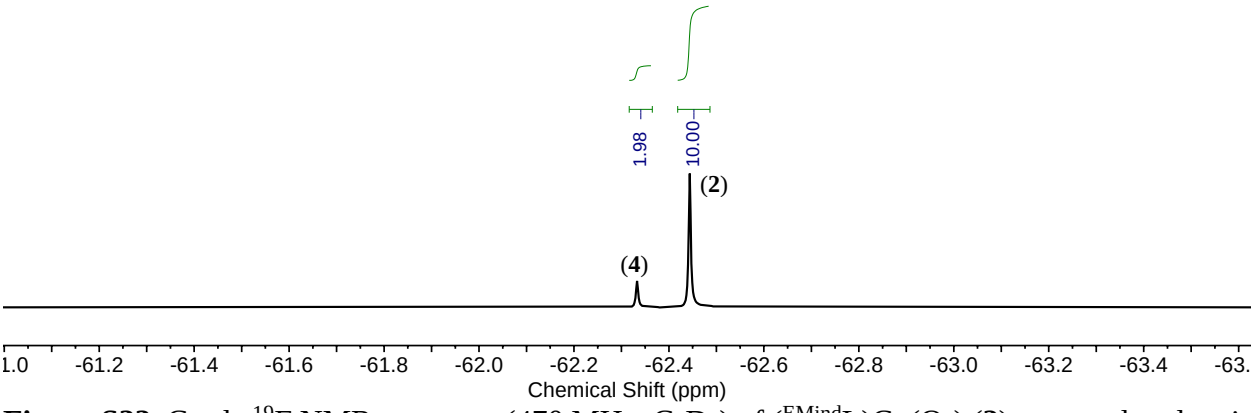

Figure S33. Crude ^{19}F NMR spectrum (470 MHz, C_6D_6) of (^{EMind}L)Cu(O_2) (**2**) prepared under air by removal of solvent from *in situ* prepared (^{EMind}L)Cu(CH_2Cl_2) (**4**). The baseline resonances denote unconverted **4** (*ca*. 17 % by integration).

Table S1. Summary of O_2 Displacement from Reagent Addition to (^{EMind}L)Cu(O_2) (**2**).

Ligand Identity	*Observation*	*% **2** after addition*	*% **2** after evacuation*
Alkanes[a]	No O_2 Displacement	100	100
Methanol[a]	No O_2 Displacement	100	100
Benzene[a]	No O_2 Displacement	100	100
Diethyl Ether[a]	No O_2 Displacement	100	100
Dioxane[a]	No O_2 Displacement	100	100
Hydrogen Gas[d]	No O_2 Displacement	100	100
Toluene[a]	Reversible O_2 Displacement	0	84
Dichloromethane[a]	Reversible O_2 Displacement	5	83
Carbon Disulfide[a]	Reversible O_2 Displacement	15	80
Cyclohexene[b]	Reversible O_2 Displacement	70	100
Thiophene[b]	Reversible O_2 Displacement	2	75
Hydroxylamine[b]	Reversible O_2 Displacement[e]	0	100
Chlorobenzene[b]	Partial O_2 Displacement	85	–[f]
1,2-Dichlorobenzene[b]	Partial O_2 Displacement	82	–[f]
Acetone[a]	Partial O_2 Displacement	80	–[f]
Dimethylsulfoxide[b]	Partial O_2 Displacement	30	–[f]
Pyrazine[c]	Irreversible O_2 Displacement	0	0
Hydrazine[c]	Irreversible O_2 Displacement	0	0
Acetonitrile[b]	Irreversible O_2 Displacement	0	0
Carbon Monoxide[d]	Irreversible O_2 Displacement	0	0
Dimethylsulfide[c]	Irreversible O_2 Displacement	0	0
Chloroform[a]	Oxidation to (^{EMind}L)CuCl	0	–[e]
Carbon Tetrachloride[a]	Oxidation to (^{EMind}L)CuCl	0	–[e]
Nitromethane[b]	Partial Demetallation	85	–[e]
1,1-Dichloroethane[b]	Partial Demetallation	80	–[e]
Tetrahydrofuran[a]	Decomposition upon vacuum	45	–[e]
Tetrachloroethylene[c]	Decomposition upon vacuum	70	–[e]
Ammonia[b]	Complete Demetallation	0	–[e]

[a]Dissolution of **2** in neat reagent with conversion recorded by ^{19}F NMR spectroscopy. Removal of solvent followed by dissolution in C_6D_6 was employed to determine regeneration of **2**. [b]100 equiv. of reagent employed to **2** in C_6D_6. [c]Stochiometric reagent added to **2** in C_6D_6. [d]1 atm added to **2** in C_6D_6. [e]Removal of hydroxylamine under reduced pressure afforded partial decomposition with formation of **2** and (^{EMind}L)H. Nonetheless, removal of hydroxylamine by slow evaporation under air under ambient conditions reafforded **2** in quantitative yield. [f]Not measured due to decomposition to low conversion or inability to remove excess ligating reagent.

Reformation of (^{EMind}L)Cu(O_2) (2) from (^{EMind}L)CuI (6).

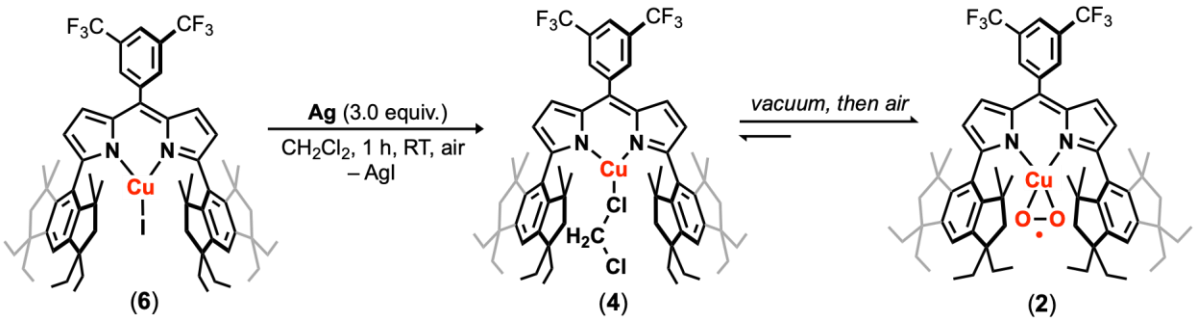

General Procedure. Treatment of (^{EMind}L)CuI (**6**) with metallic silver in dichloromethane under air afforded (^{EMind}L)Cu(CH_2Cl_2) (**4**), which could be converted into a mixture of **5** and (^{EMind}L)Cu(O_2) (**2**) upon removal of excess dichloromethane.

Note I: Chemical reduction of (^{EMind}L)CuI (**6**) with stoichiometric potassium graphite (KC_8) under N_2 in diethyl ether was able to afford (^{EMind}L)Cu(N_2) (**1**) in quantitative yield following workup, which could be converted to **2** upon air exposure. Due to the necessity to conduct the reduction under N_2 in this protocol based on the air-sensitivity of KC_8, the preparation of **2** through metallic silver under air is favored.

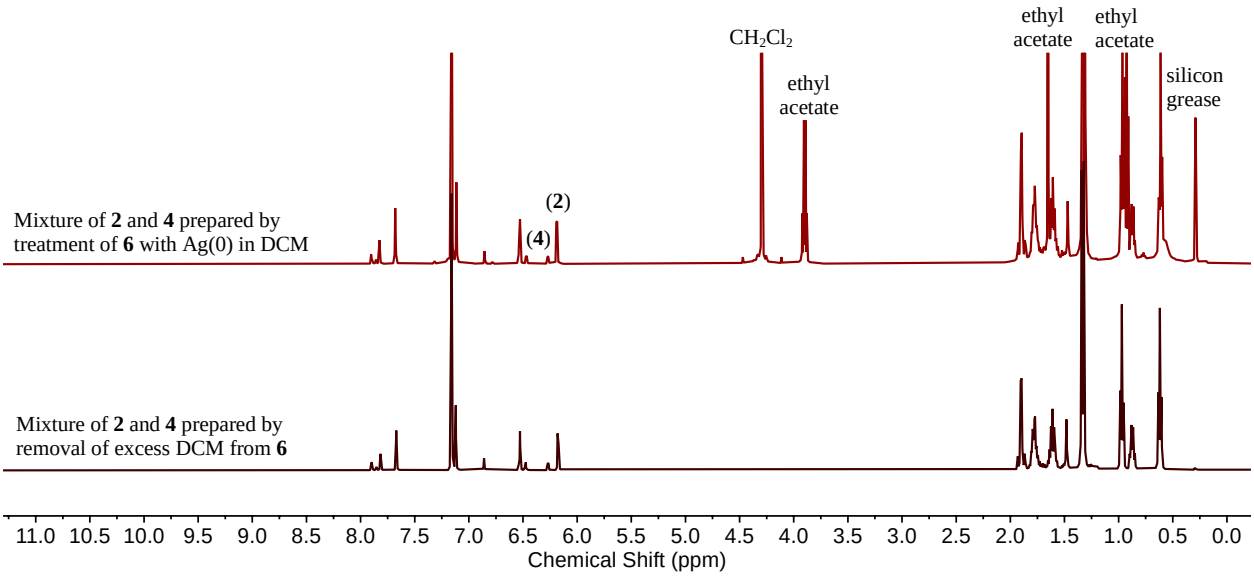

Figure S34. Comparison of ^{1}H NMR spectra (500 MHz, C_6D_6) from chemical reduction of (^{EMind}L)CuI (**6**) under air with metallic silver in dichloromethane (1 h; *top*, *red*) to a mixture of (^{EMind}L)Cu(O_2) (**2**) and (^{EMind}L)Cu(CH_2Cl_2) (**4**), (*bottom*, *maroon*).

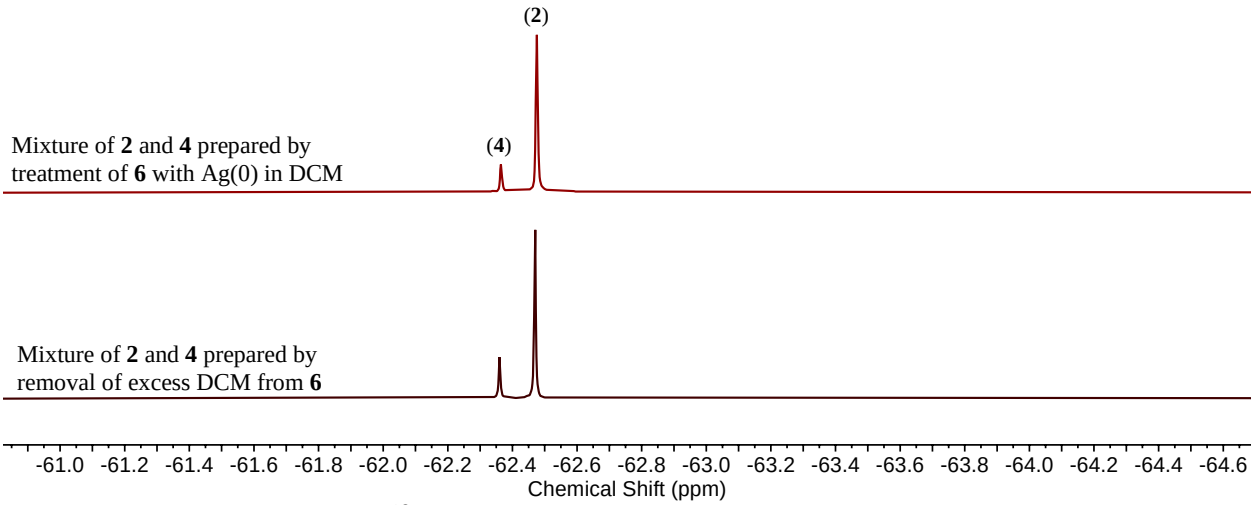

Figure S35. Comparison of ^{19}F NMR spectra (470 MHz, C_6D_6) from chemical reduction of (^{EMind}L)CuI (**6**) under air with metallic silver in dichloromethane (1 h; *top*, *red*) to a mixture of (^{EMind}L)Cu(O_2) (**2**) and (^{EMind}L)Cu(CH_2Cl_2) (**4**), (*bottom*, *maroon*).

Thermal Cycling between (^{EMind}L)Cu(N_2) (1) and (^{EMind}L)Cu(O_2) (2).

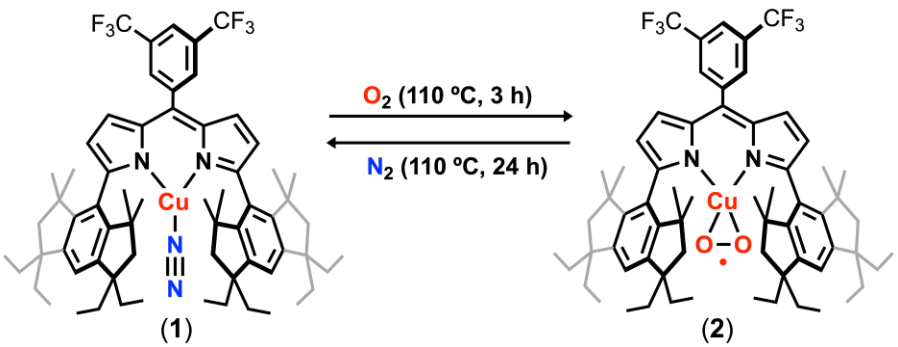

General Procedures. Under air, crystalline (^{EMind}L)Cu(O_2) (**2**) was crushed with a Teflon rod until no additional crystalline facets were apparent and the sample became a finely divided powder, noting the employment of large crystals of **2** results in slow apparent rates of gas exchange. The sample (*ca*. 10 mg) was loaded into a pre-weighed metal and loaded into a thermogravimetric analysis instrument (TGA500, TA Instruments). The initial mass was recorded, and a temperature ramp of 1 ºC/min to 110 ºC was set under active O_2 flow, followed by holding at this temperature for 24 h to ensure removal of lattice solvent. The gas stream was switched to N_2, and the sample was held at 110 ºC under N_2 flow for 24 h. The gas inlet stream was switched to O_2, and the sample was held at either 110 ºC (Figure S36) or 30 ºC (Figure S37) under O_2 flow for 3 h. During gas switching, an artifact is present by TGA due to the differences in buoyancy of the inlet gas stream (see figure) in which switching from N_2 to O_2 results in an artifact mass increase, and switching from O_2 to N_2 results in an artifact mass decrease. This cycling procedure was repeated for a total of five cycles. Once the instrument temperature was set back to room temperature, the sample was subsequently removed from the instrument and analyzed by multinuclear NMR spectroscopy to assess for decomposition.

The non-quantitative conversion of **2** into **1** is attributed to slow diffusion of N_2 into the bulk microcrystalline sample.

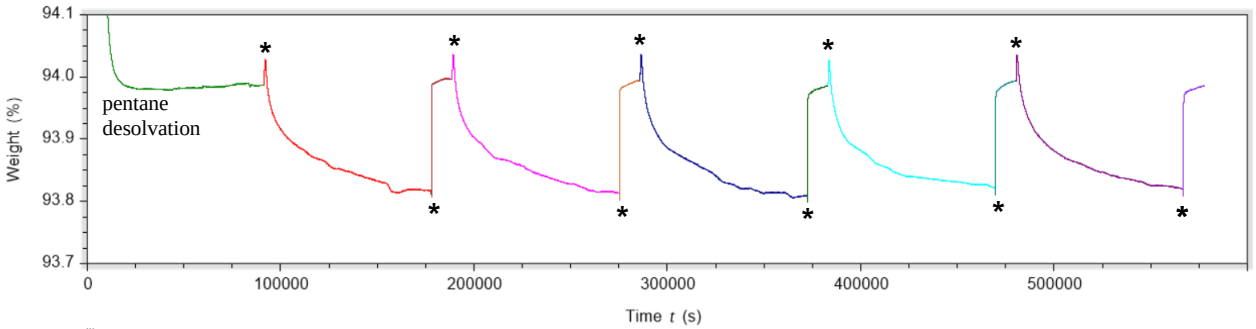

Figure S36. Uncorrected thermal gravimetric analysis (TGA) cycling of (^{EMind}L)Cu(O_2) (**2**) under alternating N_2/O_2 cycles at a constant temperature of 110 ºC. The initial mass loss prior to cycling is attributed to loss of a pentane molecule from the crystalline lattice (theoretical mass loss: 6.18 %, observed 6.02 %; difference is attributed to partial desorption of the pentane). Features marked with asterisks are instrument artifacts attributed to switching gas inlet streams.

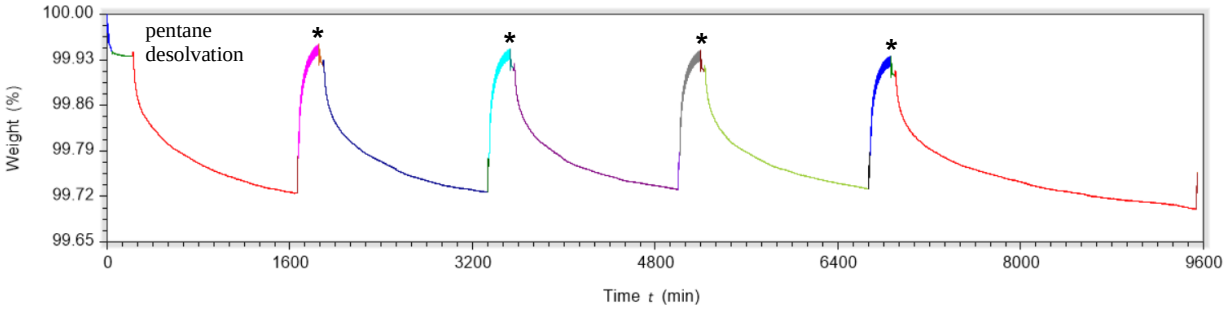

Figure S37. Uncorrected thermal gravimetric analysis (TGA) cycling of (^{EMind}L)Cu(O_2) (**2**) under alternating N_2 (110 ºC)/O_2 (30 ºC) cycles. Pre-activation of the sample by heating at 100 ºC under vacuum was conducted to remove the bulk of lattice solvent. Features marked with asterisks are instrument artifacts due to thermal pulses at 30 ºC.

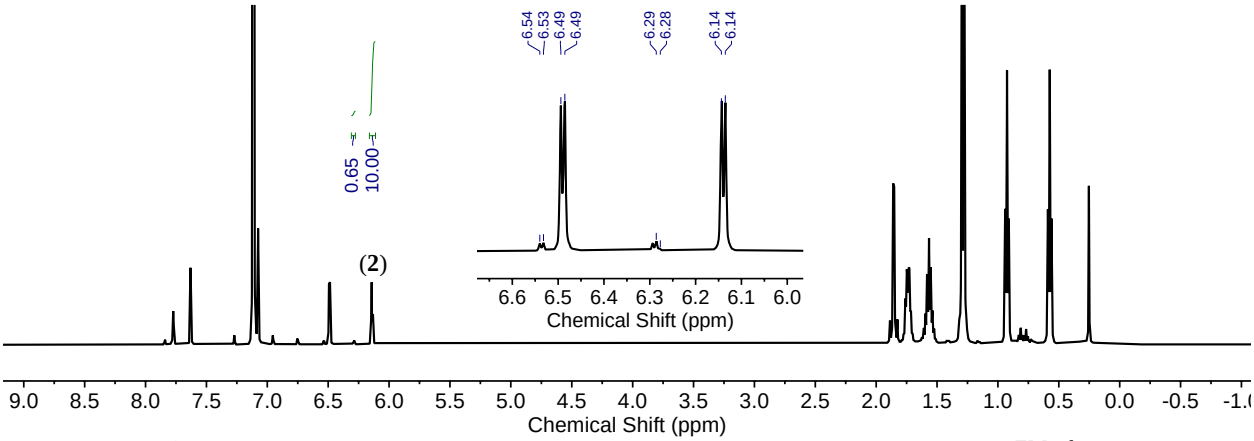

Figure S38. ^{1}H NMR spectra (500 MHz, C_6D_6) post-TGA cycling studies of (^{EMind}L)Cu(O_2) (**2**), demonstrating minor formation of a diamagnetic decomposition species (ca. 5 % yield) with **2** as the dominant species. Inset highlights dipyrrin C–*H* resonances, illustrating minor presence of a secondary species.

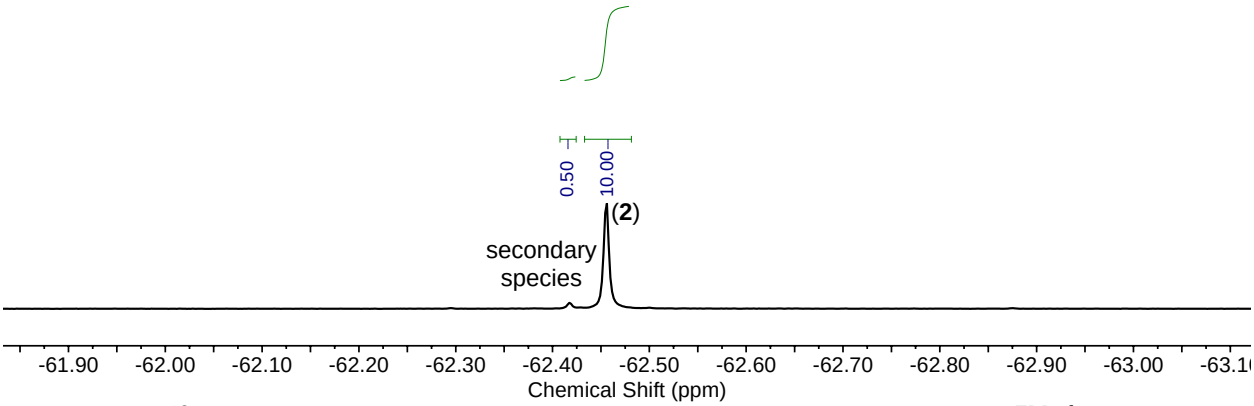

Figure S39. ^{19}F NMR spectra (470 MHz, C_6D_6) post-TGA cycling studies of (^{EMind}L)Cu(O_2) (**2**), demonstrating minor formation of a diamagnetic decomposition species (ca. 5 % yield) as identified independently by ^{1}H NMR spectroscopy.

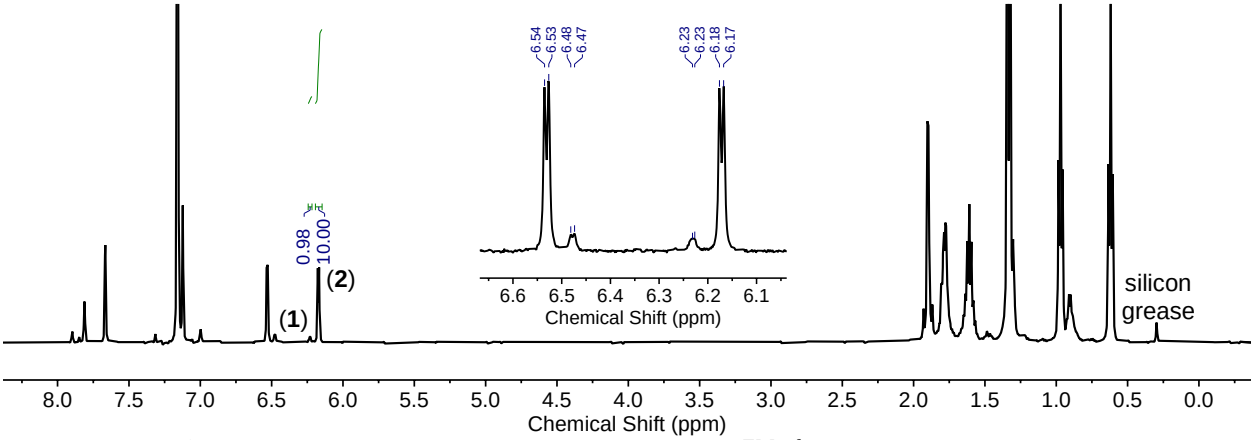

Figure S40. ^{1}H NMR spectra (500 MHz, C_6D_6) of (^{EMind}L)Cu(O_2) (**2**) under N_2, showing equilibration with N_2 to yield (^{EMind}L)Cu(O_2) (**1**) in *ca*. 9 % yield. Inset depicts dipyrrin C–*H* resonances for **1** and **2**.

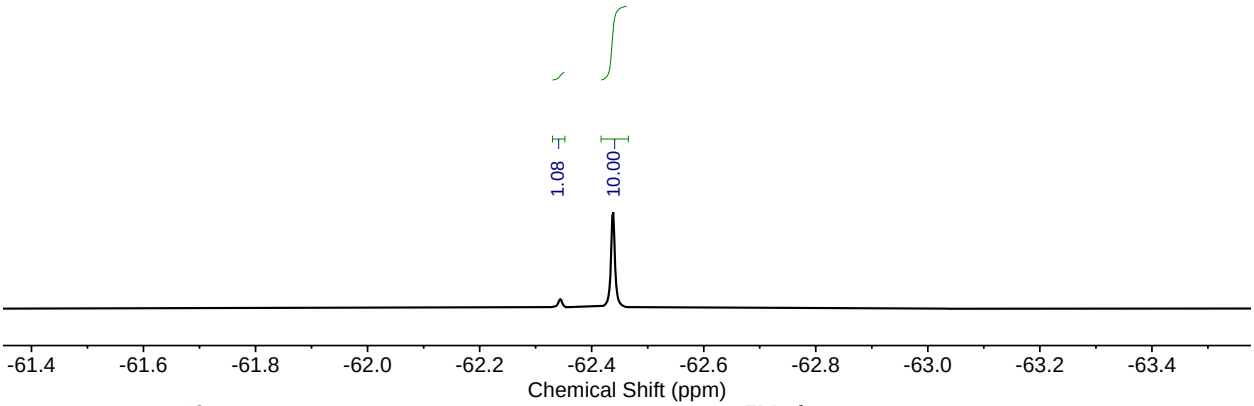

Figure S41. ^{19}F NMR spectra (470 MHz, C_6D_6) of (^{EMind}L)Cu(O_2) (**2**) under N_2, showing equilibration with N_2 to yield (^{EMind}L)Cu(O_2) (**1**) in *ca*. 10 % yield.

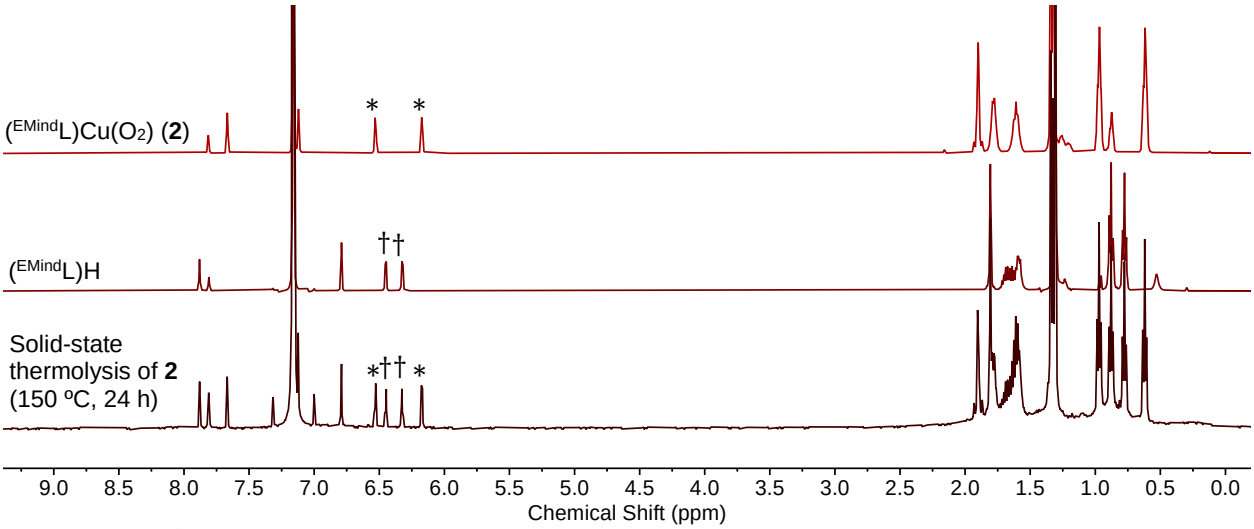

Figure S42. ^{1}H NMR spectra (500 MHz, C_6D_6) post solid-state thermolysis of **2** (150 ºC, 24 h), illustrating partial formation of (^{EMind}L)H (*ca.* 47 % yield) with partially unconverted (^{EMind}L)Cu(O_2) (**2**). Diagnostic resonances of (^{EMind}L)Cu(O_2) (**2**) are marked with an asterisk (*), and diagnostic resonances of (^{EMind}L)H are marked with an obelisk (†).

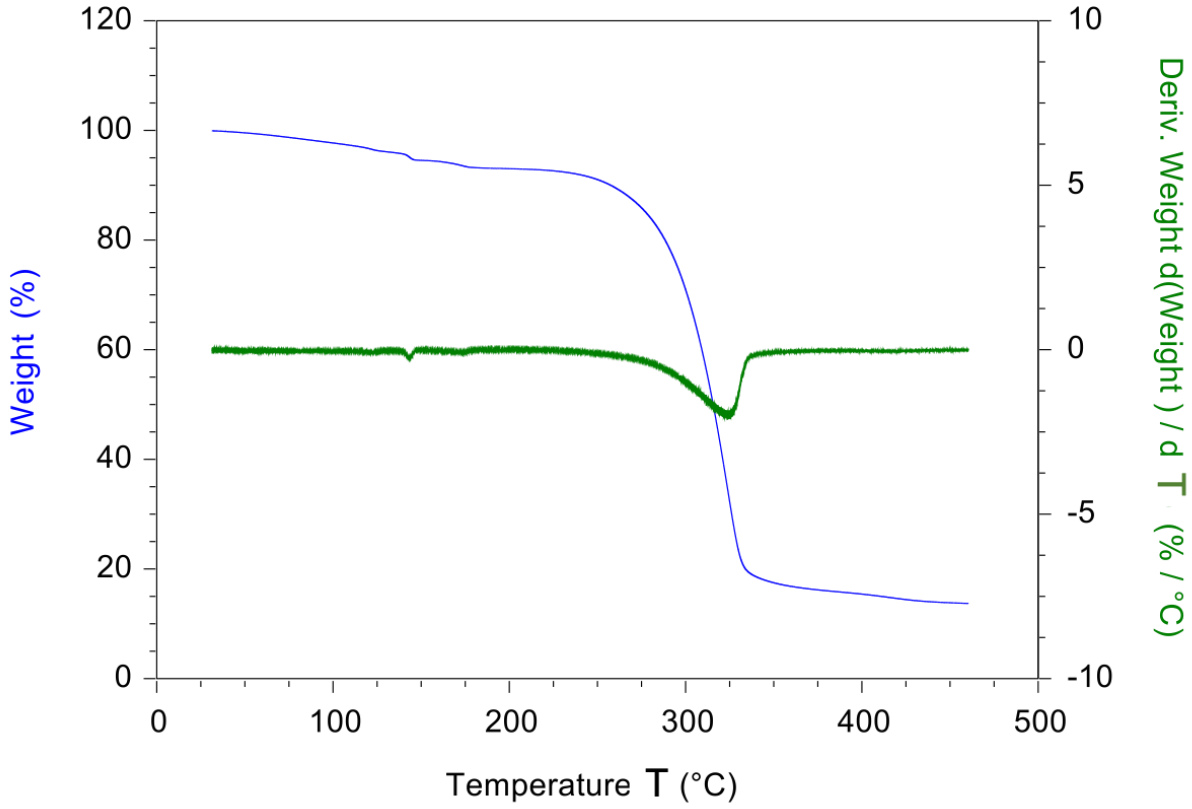

Figure S43. Thermogravimetric analysis (TGA) of crystalline (^{EMind}L)Cu(O_2) (**2**) under Ar with increasing temperature. The initial drop in mass is due to loss of pentane from the unit cell, followed by an event at 140 ºC associated with partial decomposition. Ligand decomposition is observed at *ca.* 280 ºC. The heating rate was set at 1 ºC/min.

Single-Crystal-to-Single-Crystal Transformation.

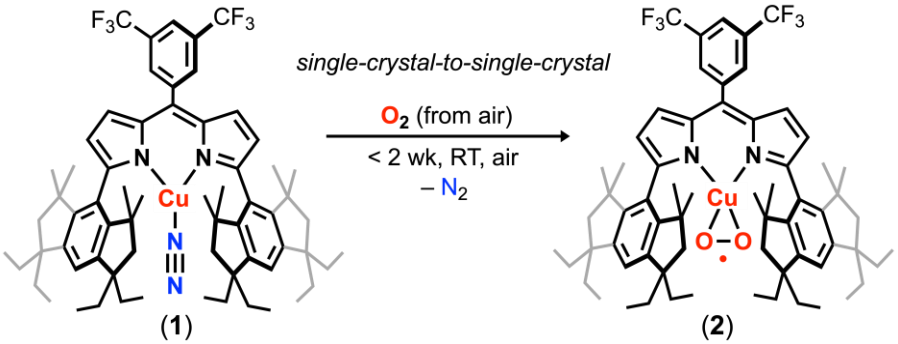

General Procedure. A dataset for a crystal of (^{EMind}L)Cu(N_2) (**1**) was collected. The crystal, kept on the MiTeGen pin with Fluorolube oil, was allowed to stand under air for two weeks, and the data set was recollected and compared to an authentic dataset of (^{EMind}L)Cu(O_2) (**2**).

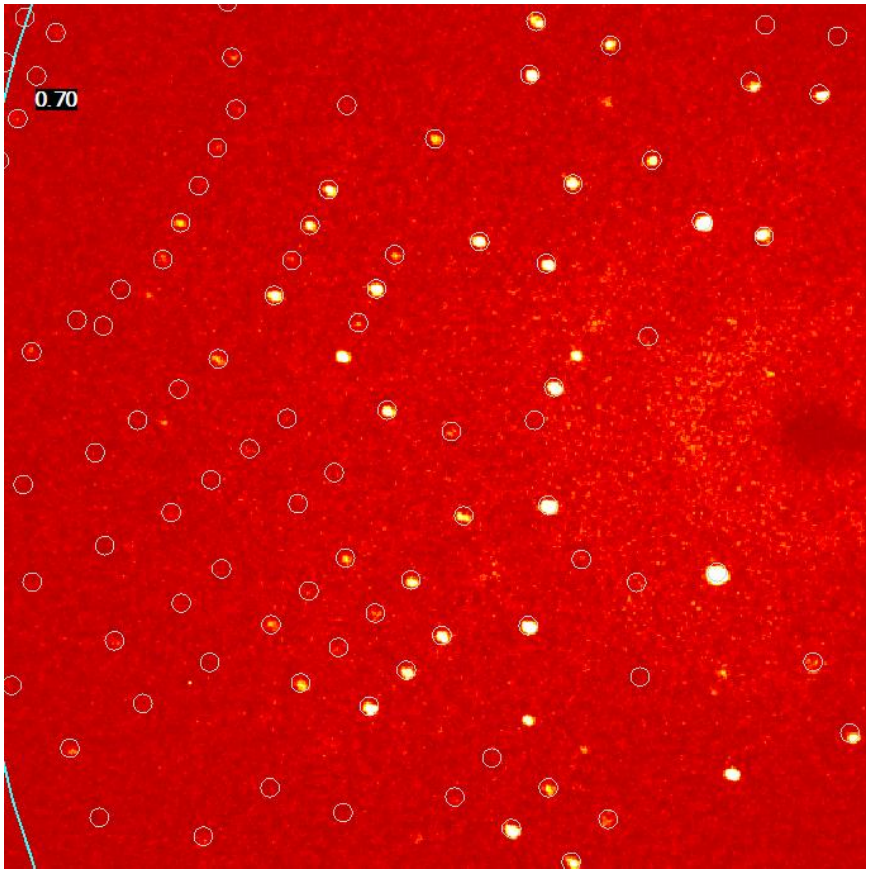

Figure S44. Single crystal of (^{EMind}L)Cu(N_2) (**1**) allowed to stand on MiTeGen pin for two weeks under air, solved as (^{EMind}L)Cu(O_2) (**2**) with no detectable electron density attributable for the N2 fragment. The above frame (2 second exposure, 0.70 Å resolution) is displayed as a reference point for the single-crystal-to-single-crystal transformation.

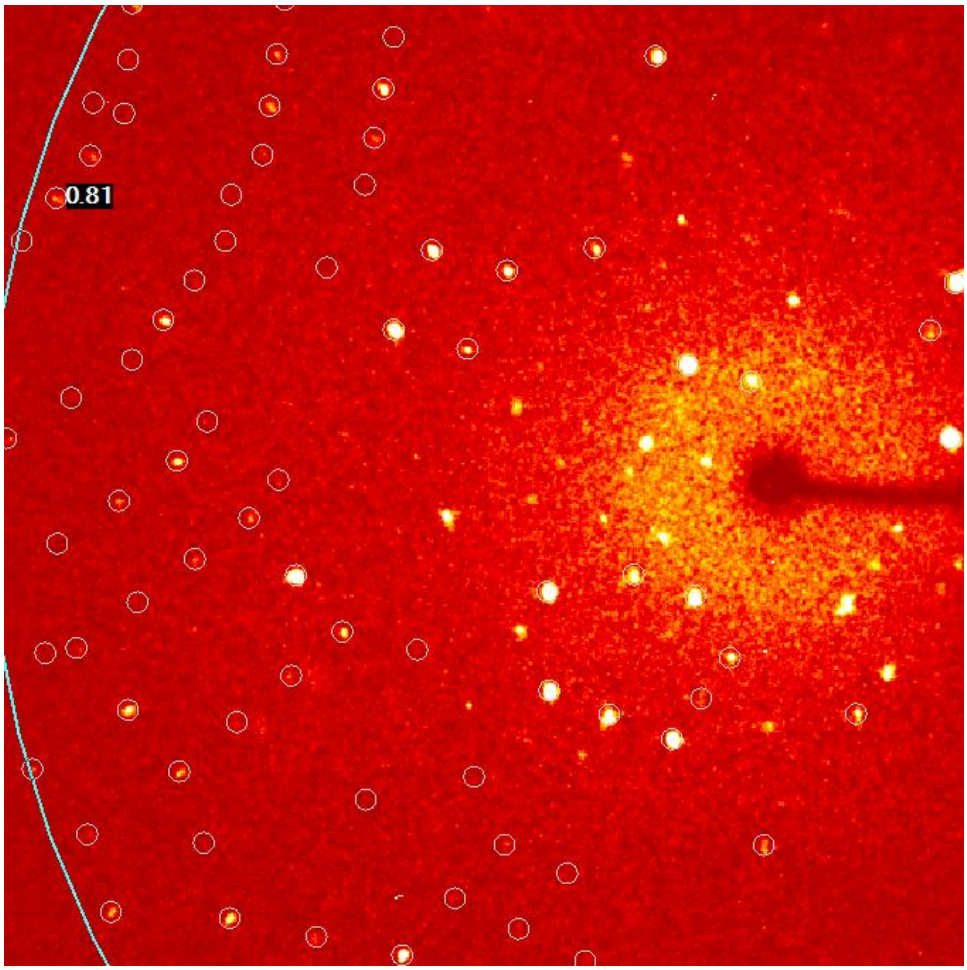

Figure S45. Single crystal of (^{EMind}L)Cu(N_2) (**1**) allowed to stand on MiTeGen pin in a vacuum desiccator for 6 days. The above frame (10 second exposure, 0.81 Å resolution) displays crystallinity preserved under prolonged vacuum exposure.

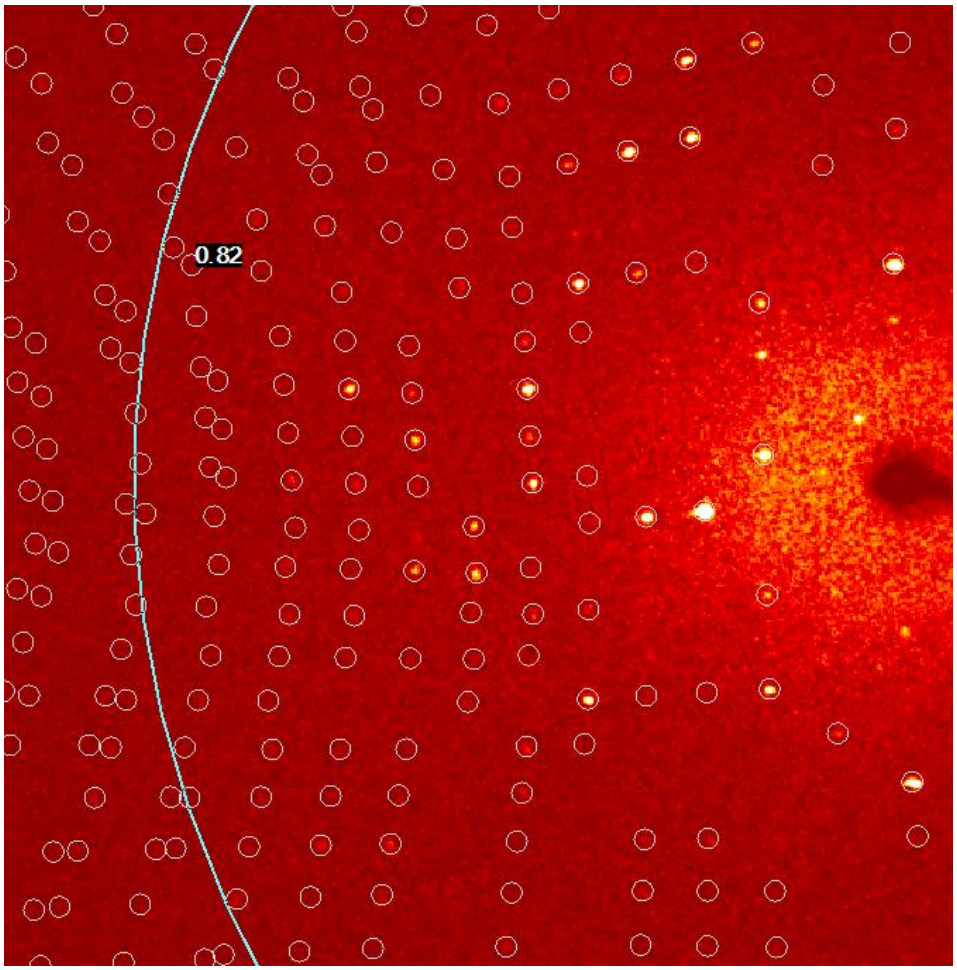

Figure S46. Single crystal of (^{EMind}L)Cu(N_2) (**1**) allowed to stand on MiTeGen pin for two weeks under air, solved as (^{EMind}L)Cu(N_2) (**2**) with no detectable electron density attributable for the N2 fragment. The above frame (1 second exposure, 0.82 Å resolution) depicts minimal degradation and preserved crystallinity.

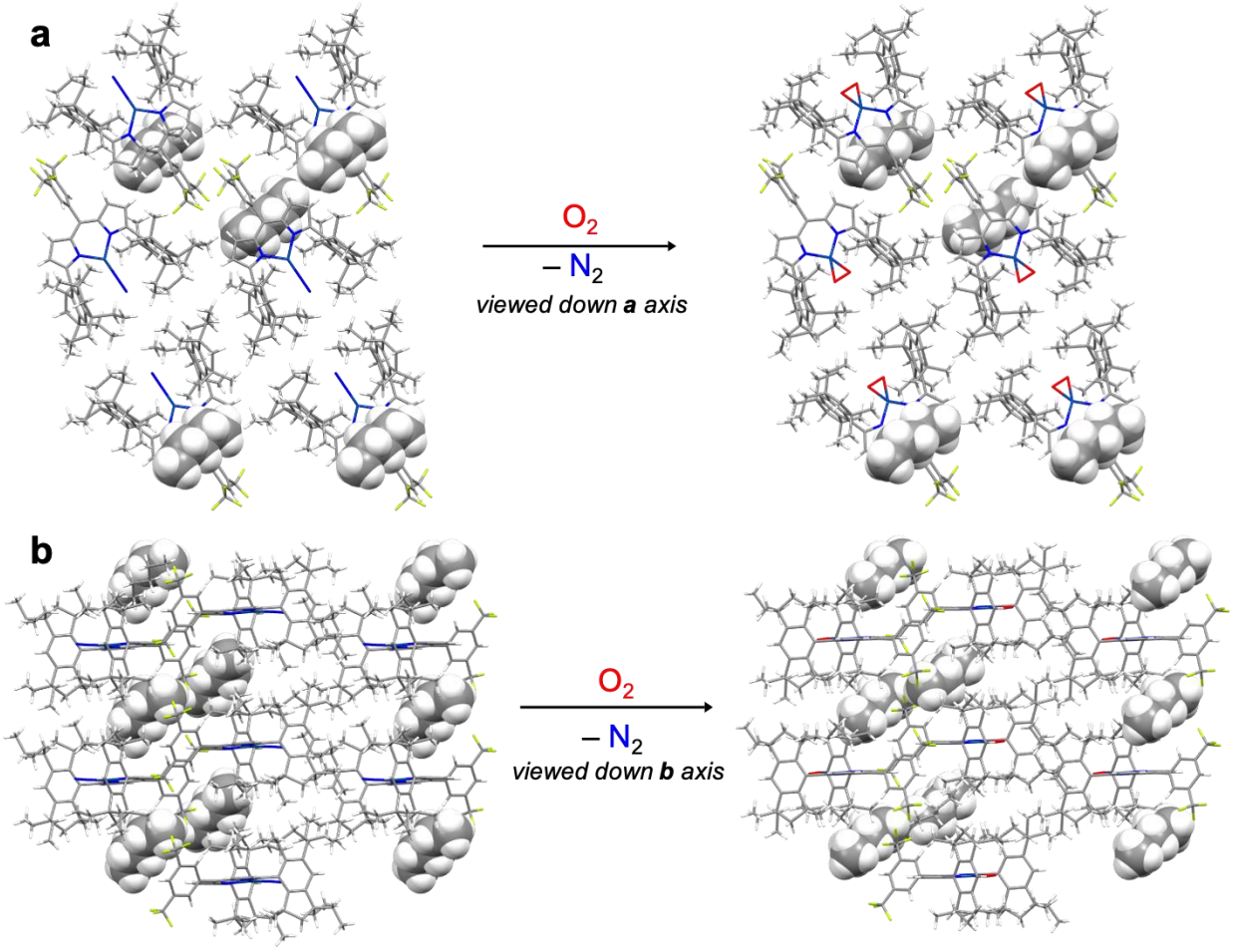

Figure S47. Depiction of pentane solvent within crystalline lattice of single-crystal-to-single-crystal conversion of (^{EMind}L)Cu(N_2) (**1**) to (^{EMind}L)Cu(N_2) (**2**). The depiction down the **a** axis (*top*) and **b** axis (*bottom*) reveal the pentane solvent molecule is spatially confined between the dipyrrin π system and the fluorinated aryl motif, resulting in low volatility under low pressure.

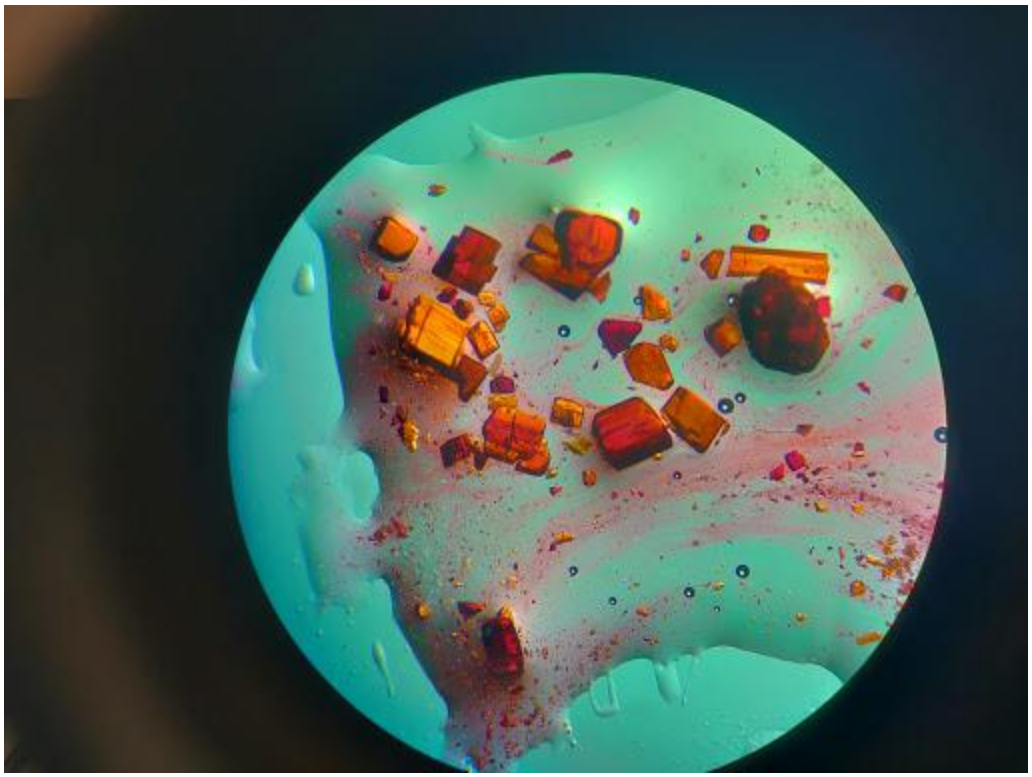

Figure S48. Snapshot of single-crystal-to-single crystal transformation (*ca*. 4 days), revealing maintained crystallinity and onset color change attributed to formation of (^{EMind}L)Cu(O_2) (**2**)

1,2-Diphenylhydrazine Oxidation with (^{EMind}L)Cu(O_2) (2) Under Air

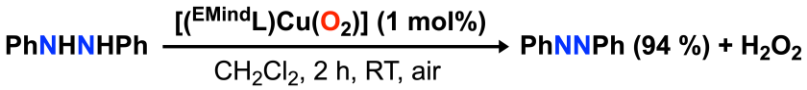

General Procedure. In a dinitrogen-filled drybox, crystalline 1,2-diphenylhydrazine was measured into a 20 mL scintillation vial. A stir bar was added, and the vial was exported from the drybox. Meanwhile, (^{EMind}L)Cu(O_2) (**2**) was measured out in air and dissolved in the appropriate solvent (*ca*. 2 mL). The scintillation vial containing the arylhydrazine was opened to air, and the stock solution of (^{EMind}L)Cu(O_2) was rapid added with stirring (1000 rpm), resulting in a rapid color change to brown-orange attributed to azoarene formation. The reaction was allowed to continue stirring without a vial cap. Aliquots were removed at the appropriate time point with removal of solvent, and the sample was dissolved in C_6D_6 and checked by multinuclear NMR spectroscopy. Control experiments, conducted in the absence of **2** with otherwise identical rapid stirring and reagent quantities, establish the paramount role of **2** in facilitating the reaction (see Fig. S49 and Note *I*).

Note I – The rapidity of 1,2-diphenylhydrazine oxidation was observed to be highly sensitive to speed of stirring and shape of reaction vessel, attributed to rate of solution oxygenation. In accord, reactions set up in NMR tubes were prohibitively slow with constant inversion of the tube (attributed to poor O_2 diffusion into solution based on minimal exposure of surface area of the solution to air), hindering a detailed kinetic analysis.

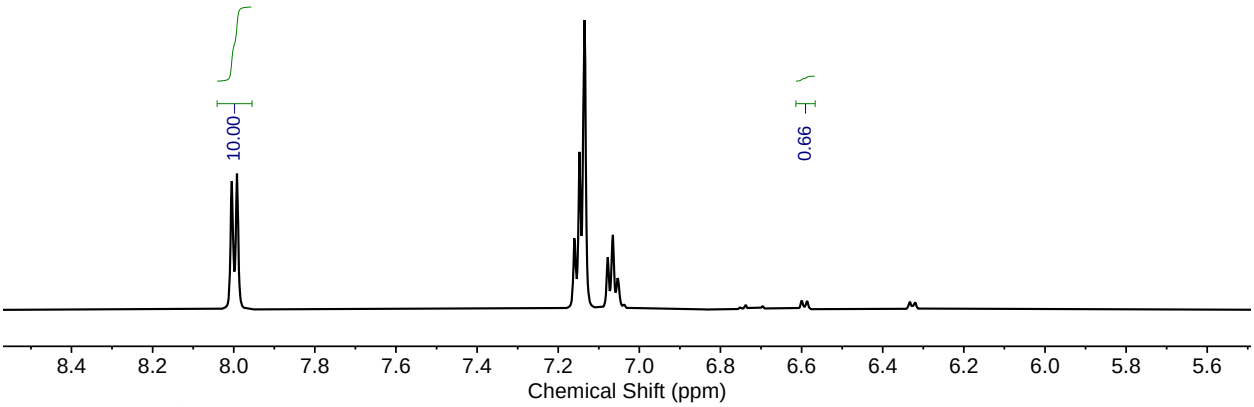

Figure S49. ^{1}H NMR spectrum (600 MHz, C_6D_6) of 1,2-diphenylhydrazine oxidation due to formation of (^{EMind}L)Cu(O_2) (**2**) in dichloromethane after 2 h. Baseline resonances correspond to dipyrrin species.

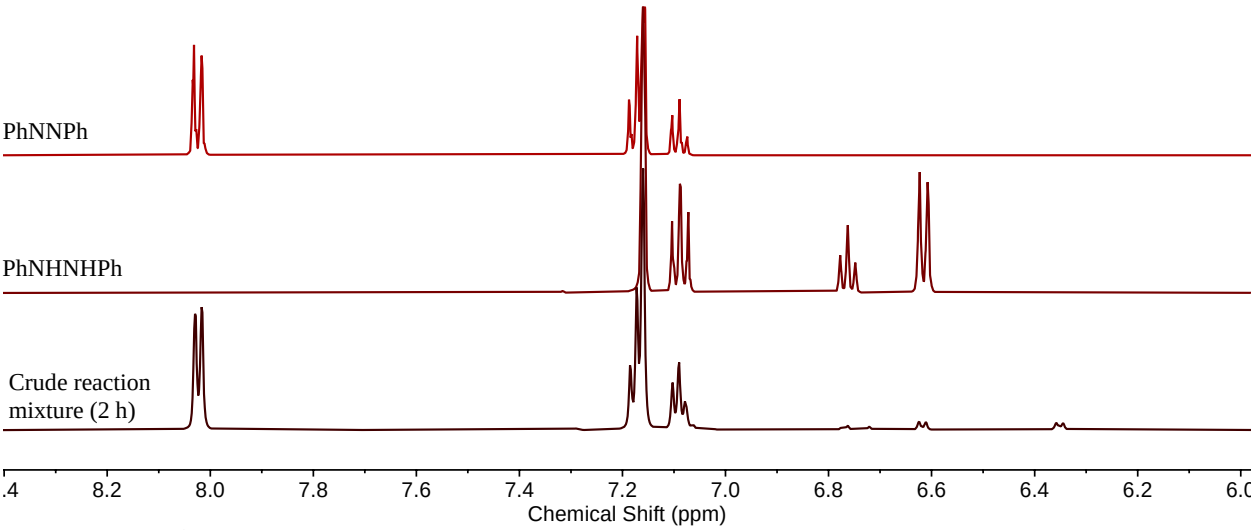

Figure S50. ^{1}H NMR spectrum (600 MHz, C_6D_6) of 1,2-diphenylhydrazine oxidation due to formation of (^{EMind}L)Cu(O_2) (**2**) in dichloromethane after 2 h.

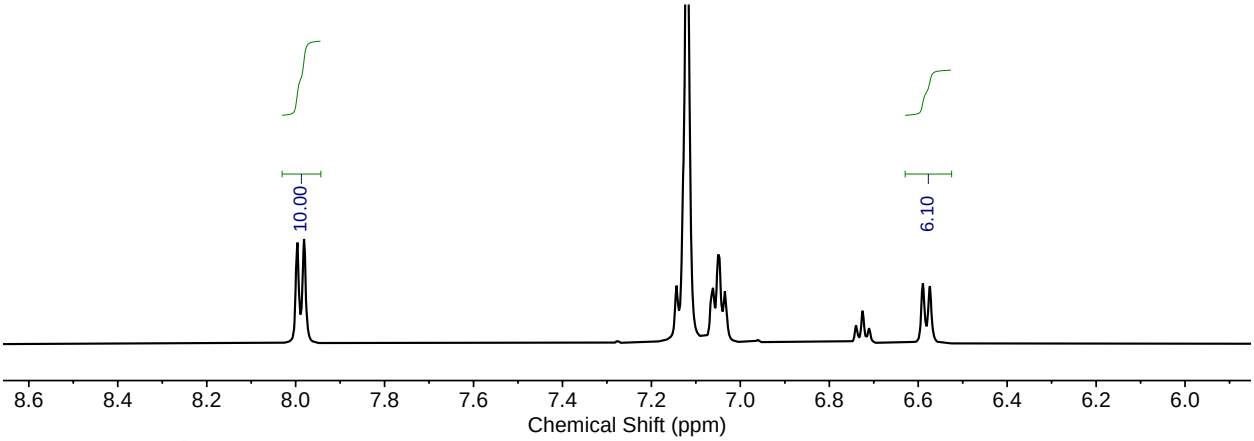

Figure S51. ^{1}H NMR spectrum (500 MHz, C_6D_6) of 1,2-diphenylhydrazine oxidation due to formation of (^{EMind}L)Cu(O_2) (**2**) in hexanes after 2 h.

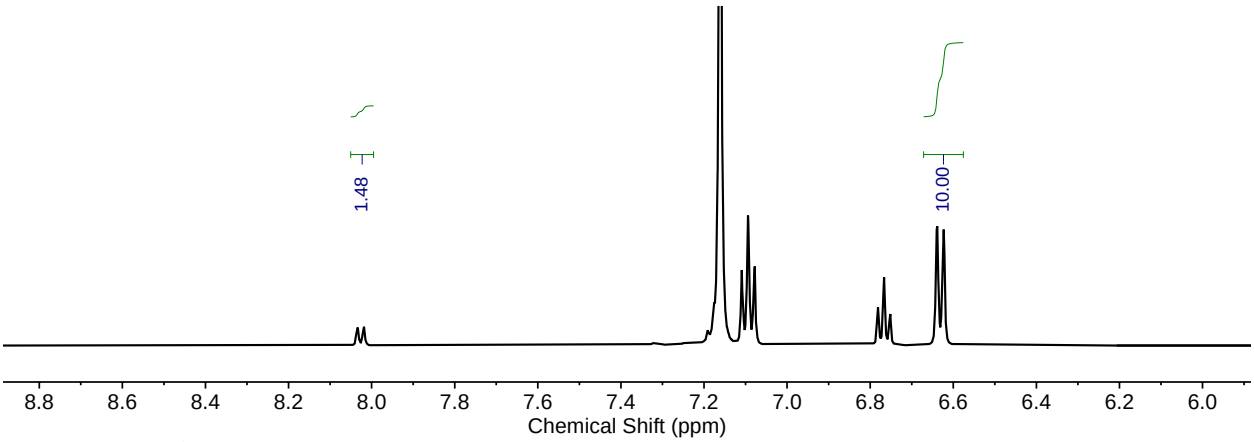

Figure S52. ^{1}H NMR spectrum (500 MHz, C_6D_6) of 1,2-diphenylhydrazine auto-oxidation in dichloromethane in the absence of (^{EMind}L)Cu(O_2) (**2**) after 2 h, revealing minor conversion to azoarene (*ca*. 13 % yield).

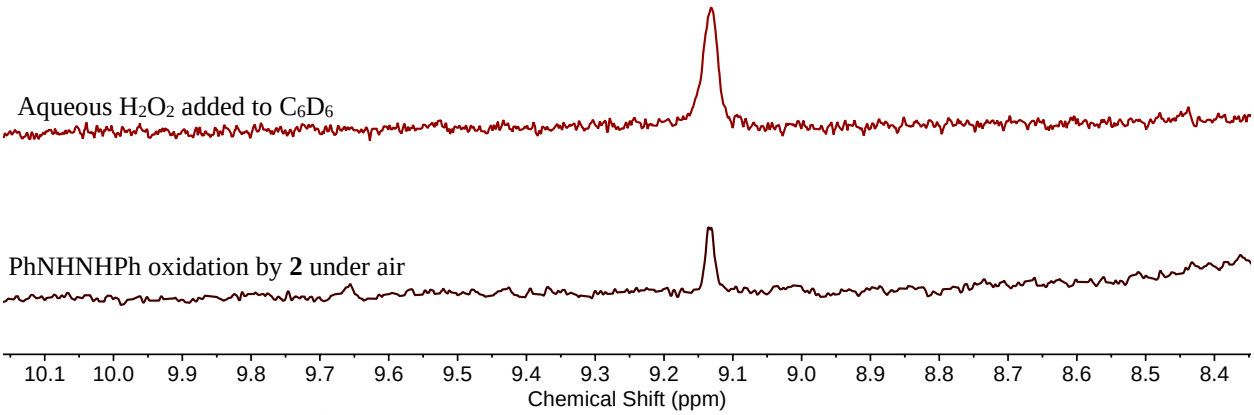

Figure S53. Truncated ^{1}H NMR spectra overlay (500 MHz, C_6D_6) of H_2O_2 in C_6D_6 (*top*, *red*) juxtaposed to crude 1,2-diphenylhydrazine oxidation (*bottom*, *maroon*), demonstrating H_2O_2 production. Due to the poor solubility of H_2O_2 in C_6D_6 and loss of H_2O_2 during workup step involving evacuation, quantification of H_2O_2 by ^{1}H NMR spectroscopy was not conducted.

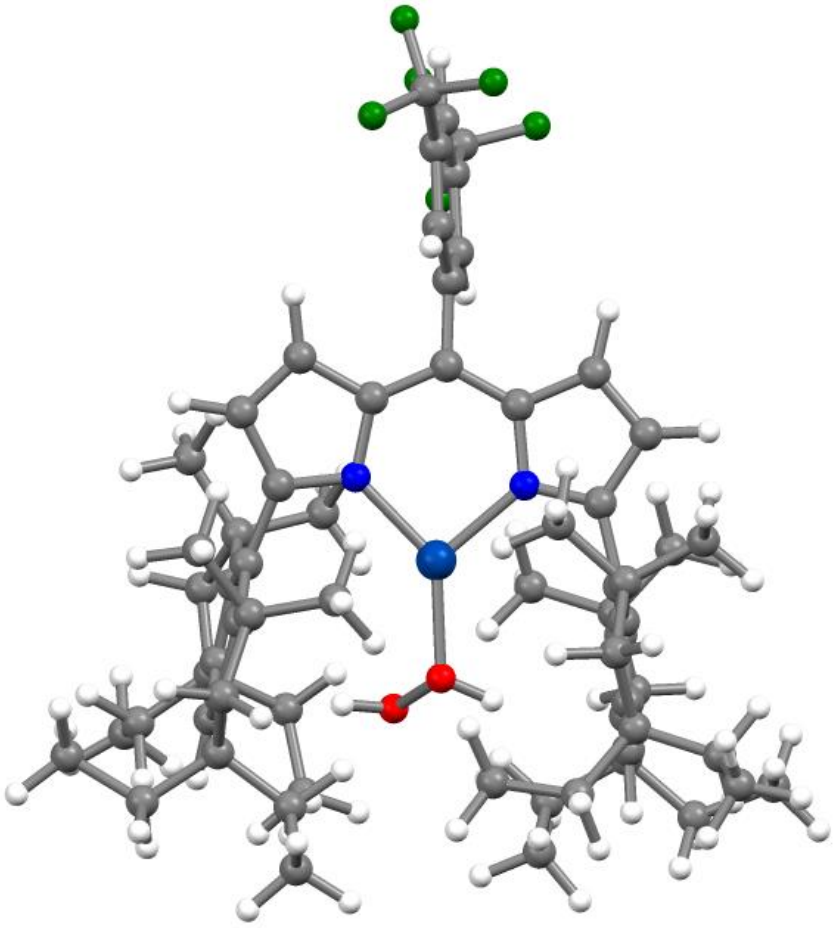

Figure S54. Geometry optimized structure of (^{EMind}L)Cu(H_2O_2) (**7**) with basis set/functional pairing lacv3p**/B3LYP–d3.[6-10] Computations were conducted with the software *Jaguar*.[11] Successful ground-state optimizations were assessed by the absence of negative frequencies and by the forces on the all atoms residing below 10^{-5} hartrees/bohr as well as total energy remaining unchanged by 10^{-4} between the final SCF iterations. Color Scheme: Cu (cobalt blue), F (green) N (blue), O (red). Geometry of (^{EMind}L)Cu(O_2) (**2**) was employed for initial coordinates.

Pertinent bond metrics include the following, which are in agreement with a cuprous ion in the dipyrrin framework with an unactivated hydrogen peroxide motif:
Cu–$N_{dipyrrin}$: 1.997 Å, 1.998 Å
Cu–O: 2.034 Å
O–O: 1.471 Å (crystalline hydrogen peroxide, $d_{O-O:}$ 1.453(7) Å)[12]
Σ(∠Cu): 360 º

Cartesian Coordinates (x,y,z) – Optimization of (^{EMind}L)Cu(H_2O_2) (**7**)

Cu1	4.410110	7.361436	16.594389
F2	7.405112	1.153821	10.874097
F3	1.426011	2.234660	10.999123
F4	8.011450	3.140978	10.233004
F5	8.216287	2.573080	12.321695
N6	4.776037	7.669791	14.655753
F7	2.125394	3.375386	9.286696
F8	2.779040	1.315507	9.553522
C9	3.793740	4.918508	18.698532
C10	6.267951	3.919119	18.761608
C11	7.418580	2.456356	11.237449
C12	2.829969	5.670000	19.406300
C13	7.850808	13.739378	16.264208
H14	8.468954	13.275910	15.487411
H15	8.205877	14.767121	16.396055
H16	6.826072	13.781666	15.884068
C17	1.403875	6.057064	18.989836
C18	5.139232	10.014306	14.975759
C19	4.527679	4.410795	12.751843
C20	5.967577	2.491439	18.267862
H21	6.910164	1.943927	18.146947
H22	5.452766	2.488530	17.307230
H23	5.351419	1.945449	18.990971
C24	3.443510	3.453537	15.309607
H25	3.295710	2.709504	14.540023
C26	6.782768	4.968684	21.000224
C27	5.118961	7.307800	12.424210
H28	5.187602	6.804889	11.469266
C29	7.173275	3.823011	20.028088
H30	6.977403	2.862732	20.521065
H31	8.236069	3.833924	19.764154
C32	4.355509	5.364636	13.892347
C33	1.649169	11.463897	15.385341
H34	0.946836	12.043374	14.778394
H35	1.041584	10.793836	16.001761
C36	7.692889	6.211170	20.743917
H37	8.737131	5.888294	20.840839
H38	7.566685	6.520204	19.702264
C39	3.876884	11.685090	16.229773

C40	3.911075	4.793123	15.103036
N41	3.968531	5.428945	16.343191
C42	8.487527	10.630238	16.671862
H43	9.188069	10.069385	17.297839
H44	9.095897	11.290484	16.045652
C45	3.675489	2.951911	11.017975
C46	4.755666	6.693975	13.668468
C47	7.922921	12.970792	17.589097
H48	7.295503	13.482095	18.332520
H49	8.947883	13.017107	17.977220
C50	3.455719	3.914262	12.009506
H51	2.448177	4.259616	12.217121
C52	4.991507	11.971766	17.017419
H53	4.935225	12.721299	17.803212
C54	6.269741	10.315258	15.766838
C55	5.120034	8.825875	14.083615
C56	2.684073	13.806636	15.727323
H57	3.463729	14.316421	16.309243
H58	3.079049	13.724139	14.707949
C59	3.600899	4.538273	17.272607
C60	8.244290	4.120249	22.967137
H61	8.695951	3.352367	22.329355
H62	8.201280	3.721038	23.985993
H63	8.921544	4.980650	22.979485
C64	2.007493	7.008437	21.266700
C65	5.339592	8.650264	12.684454
H66	5.628778	9.420920	11.982608
C67	6.187462	11.293760	16.771322
C68	2.518960	12.368326	16.303535
O69	4.474103	8.713903	18.111953
H70	4.922963	9.555498	17.893191
C71	6.959205	4.704993	17.622081
H72	7.900689	4.214457	17.347623
H73	7.182756	5.734430	17.910688
H74	6.321259	4.751274	16.738127
C75	4.395743	5.996017	21.249824
H76	4.618701	6.421633	22.223593
C77	3.938423	10.715961	15.218629
C78	5.821463	3.940623	12.482819
H79	6.657484	4.309684	13.066186

C80	6.844102	4.504998	22.475525
H81	6.437418	5.287483	23.127869
H82	6.169012	3.646122	22.584044
C83	5.348112	5.242787	20.563657
O84	5.350943	8.202373	19.176951
H85	4.732139	7.585970	19.617055
C86	1.420972	14.674226	15.713105
H87	1.620501	15.628358	15.214037
H88	1.068896	14.900166	16.724293
H89	0.599258	14.189046	15.175138
C90	8.292586	9.622323	14.347407
H91	8.276262	10.612253	13.877676
H92	7.764717	8.925952	13.692293
H93	9.337407	9.297205	14.417304
C94	3.138913	6.189076	20.670646
C95	3.226318	3.303486	16.666638
H96	2.883392	2.420780	17.187537
C97	4.954650	2.467004	10.767814
H98	5.114060	1.698310	10.020927
C99	2.592687	10.602467	14.486690
C100	5.047737	4.684016	19.308145
C101	7.337366	10.913258	18.964916
H102	7.094834	9.847783	18.899727
H103	6.464683	11.395329	19.427911
C104	7.498526	11.479452	17.523626
C105	6.027049	2.966353	11.509374
C106	1.392862	7.076292	17.827208
H107	2.017734	7.946055	18.052243
H108	0.370569	7.430084	17.647175
H109	1.762899	6.626276	16.903204
C110	7.633135	8.240783	16.342767
H111	8.654060	7.851161	16.435449
H112	7.065294	7.561159	15.703588
H113	7.175749	8.219785	17.336789
C114	1.955265	12.443708	17.745871
H115	2.512935	13.209163	18.303444
H116	0.922044	12.807923	17.688850
C117	7.462249	7.434116	21.636014
H118	6.453220	7.838179	21.515308
H119	8.160683	8.232325	21.363069

H120	7.616022	7.210237	22.696951
C121	0.563199	4.829714	18.591038
H122	0.939792	4.368840	17.674536
H123	-0.478245	5.126497	18.419661
H124	0.575084	4.073233	19.383626
C125	1.978396	11.133705	18.541353
H126	2.998280	10.781641	18.716265
H127	1.444559	10.326988	18.028073
H128	1.499989	11.270123	19.515754
C129	2.502021	2.461858	10.211301
C130	7.663989	9.670699	15.751742
C131	2.713823	11.200417	13.066457
H132	1.737586	11.191576	12.566821
H133	3.410078	10.614117	12.459574
H134	3.072408	12.234152	13.092585
C135	0.829755	6.707516	20.293469
H136	0.256694	7.610103	20.061639
H137	0.128734	6.012700	20.765484
C138	8.548012	11.082858	19.889926
H139	9.454778	10.647600	19.454850
H140	8.367189	10.578397	20.844891
H141	8.756233	12.134907	20.108095
C142	2.025828	9.171686	14.380325
H143	2.087525	8.649262	15.340444
H144	2.554352	8.569754	13.640093
H145	0.971176	9.223308	14.082993
C146	2.431248	8.507458	21.226447
H147	3.395197	8.604195	21.745163
H148	2.621381	8.784253	20.182478
C149	1.683624	6.581951	22.722470
H150	0.751735	7.074815	23.025898
H151	2.464257	6.976845	23.387469
C152	1.554488	5.070254	22.949394
H153	0.797250	4.622172	22.296374
H154	1.262692	4.859783	23.983827
H155	2.499890	4.555081	22.753973
C156	1.437688	9.498823	21.839561
H157	0.457645	9.445904	21.352511
H158	1.805433	10.523745	21.726915
H159	1.289592	9.319771	22.908868

Table S2. X-ray diffraction experimental details.[a]

	(^{EMind}L)Cu(η^2-C_6H_6) (**1-benzene**) – 2049910	(^{EMind}L)Cu(O_2) (**2**) – 2049906	(^{EMind}L)Cu(CH_2Cl_2) (**4**) – 2049909	(^{EMind}L)Cu(NH_2NH_2) (**5**) – 2049908	(^{EMind}L)CuI (**6**) – 2049907
Moiety Formula	$C_{71}H_{87}CuF_6N_2 \bullet C_6H_6$	$C_{65}H_{81}CuF_6N_2O_2 \bullet C_5H_{12}$	$C_{66}H_{81}Cl_2Cu_2N_2 \bullet C_5H_{12}$	$C_{65}H_{85}CuF_6N_4 \bullet C_5H_{12}$	$C_{65}H_{81}CuF_6IN_2$
FW	1296.29	1172.02	1222.93	1172.07	1194.77
***λ* (nm)**	0.71073	0.71073	0.71073	0.71073	0.71073
***T* (K)**	100(2)	100(2)	100(2)	100(2)	100(2)
Crystal System	Triclinic	Triclinic	Triclinic	Triclinic	Triclinic
Space Group (*Z*)	$P\bar{1}$ (2)	$P\bar{1}$ (2)	$P\bar{1}$ (2)	$P\bar{1}$ (2)	$P\bar{1}$ (2)
***a* (Å)**	14.0750(8)	10.415(2)	10.757(12)	10.514(4)	10.546(4)
***b* (Å)**	14.2433(8)	13.866(3)	14.73(2)	13.806(3)	13.838(6)
***c* (Å)**	17.2305(10)	22.041(5)	22.63(2)	22.372(5)	22.418(8)
***α* (°)**	93.596(1)	94.705(4)	93.90(4)	82.714(14)	97.302(8)
***β* (°)**	103.655(1)	93.341(5)	99.65(3)	89.690(15)	90.014(8)
***γ* (°)**	99.936(1)	97.663(4)	96.60(5)	82.004(11)	97.506(8)
Volume (Å^3)	3286.9(3)	3136.3(12)	3498(7)	3189.7(16)	3217(2)
Calc. *ρ* (mg/m^3)	1.237	1.241	1.161	1.220	1.233
***μ* (mm^{-1})**	0.394	0.412	0.444	0.403	0.874
Crystal Size (mm)	0.16x0.22x0.23	0.13x0.22x0.24	0.17x0.22x0.23	0.10x0.10x0.20	0.12x0.15x0.40
Reflections	8322	7017	6913	7366	6338
Completeness (to 2*θ*)	0.990	0.960	0.960	0.984	0.992
GOF on F^2	1.068	1.027	1.039	1.029	0.973
R1, *w*R2[a] [*I* > 2*σ*(*I*)]	0.0469, 0.1311	0.0641, 0.1685	0.0879, 0.2803	0.0663, 0.1391	0.0778, 0.1975

[a] $R1 = \sum||F_o| - |F_c||/\sum|F_o|$, $wR2 = \{\sum[w(F_o^2 - F_c^2)^2]/\sum[w(F_o^2)^2]\}^{1/2}$

X-Ray Diffraction Techniques. All structures were collected on a Bruker three-circle platform goniometer equipped with an Apex II CCD and an Oxford cryostream-cooling device fixed at 100 K. Radiation was from a graphite fine focus sealed tube Mo Kα (λ = 0.71073 Å) source (**1-benzene, 2, 3, 4, 5, 6**). The partial solubility of all complexes on the (^{EMind}L) platform in Paratone–*N* oil forced us to employ an alternative crystal mounting procedure. Crystals were suspended in minimal thawing Fluorolube (stored in a vacuum desiccator or the drybox to minimize water content), quickly transferred to a dry ice bath outside the drybox (< 10 seconds transit time) and rapidly transferred to a room temperature microscope slide (*ca*. 3 minute transit time) for crystal selection with a glass fiber pin. At room temperature, crystals were observed to darken rapidly and lose the ability to polarize incidental light, attributed to desolvation of the unit cell and gradual dissolution into the surrounding oil. Such behavior was common for crystals isolated from slow cooling of concentrated hydrocarbon solutions, pentane in particular. Consequently, the crystal selection process was rapidly conducted at low temperatures, considering crystal size and crystal quality. For **1-benzene** and **4**, rapid degradation of the crystals was observed under ambient conditions due to the heightened sensitivity to O_2 and N_2. None of the crystals shows significant decay during the data collection.

Data was collected as a series of φ and/or ω scans. Data integration down to 0.84 Å resolution was carried out using SAINT V8.37 A[13] with reflection spot size optimization. Absorption corrections were made with the program SADABS.[14] Space group assignments were determined by examination of systematic absences, E-statistics, and successive refinement of the structures. The structure was solved by the Intrinsic Phasing methods and refined by least-squares methods against F^2 using SHELXT-2014[15] and SHELXL-2014[16] with the OLEX2 interface.[17] The program PLATON was employed to confirm the absence of higher symmetry space groups.[18] All non-H atoms, including the disorder fragments, were located in difference Fourier maps, and then refined anisotropically. The restraints on bond lengths and constraints of the atomic displacement parameters on each pair of disorder fragments (SADI/SAME and EADP instructions of SHELXL-2014)[16] as well as the restraints of the atomic displacement parameters (SIMU/RIGU instructions of SHELXL-2014), if necessary, have been applied for the disorder refinement.[19] All non-hydrogen atoms were refined anisotropically. Outlier reflections were omitted from refinement when appropriate. Hydrogen atoms on C atoms were placed at idealized positions and refined using a riding model. The isotropic displacement parameters of all hydrogen atoms were fixed to 1.2 times the atoms they are linked to (1.5 times for methyl groups). Crystallographic refinement details, including disorder modeling and software employed, have been delineated within in each crystallographic information file (**.cif*).

Molecular graphics were generated using Povray V3.7.[20]

Further details on particular structures are noted below:

(^{EMind}L)Cu(η^2-C_6H_6) (1-benzene). The structure was solved in the triclinic space group $P\bar{1}$ with one molecule of copper-containing complex per asymmetric unit and two molecules per unit cell. One molecule of pentane was located and modelled appropriately. Positional disorder of the benzene ligand (C66–C71) over two positions was observed, which was modelled using similarity constraints and restraints. CCDC Identifier: 2049910.

(^{EMind}L)Cu(O_2) (2). The structure was solved in the triclinic space group $P\bar{1}$ with one molecule of copper-containing complex per asymmetric unit and two molecules per unit cell. One molecule of pentane was positionally disordered and modelled using similarity constraints and restraints. One of the trifluoromethyl substituents containing C17 was positionally and rotationally disordered and subsequently modelled using similarity constraints and restraints. Several reflects were co-incidental with the beam-stop and omitted. CCDC Identifier: 2049906.

(^{EMind}L)Cu(CH_2Cl_2) (**4**). The structure was solved in the triclinic space group $P\bar{1}$ with one molecule of copper-containing complex per asymmetric unit and two molecules per unit cell. One molecule of pentane was located and modelled appropriately using the RIGU command. A second molecule of pentane was disordered about a special position and squeezed out using the Olex2 mask function to improve the C–C bond precision. The ligated molecule of dichloromethane was disordered over two positions and modelled using similarly constraints and restraints. CCDC Identifier: 2049909

(^{EMind}L)Cu(NH_2NH_2) (**5**). The structure was solved in the triclinic space group $P\bar{1}$ with one molecule of copper-containing complex per asymmetric unit and two molecules per unit cell. Positional disorder of an ethyl motif containing C55 was modeled using similarity constraints and restraints. The trifluoromethyl motif containing C16 was positionally and rotationally disordered, modelled using similarity constraints and restraints. The hydrazine motif containing N3 was disordered over two positions and modelled appropriately. One molecule of pentane was located and modelled appropriately. CCDC Identifier: 2049908.

(^{EMind}L)CuI (**6**). The structure was solved in the triclinic space group $P\bar{1}$ with one molecule of copper-containing complex per asymmetric unit and two molecules per unit cell. Positional disorder within the hydrindacene motif containing C58 was modeled using similarity constraints and restraints. One molecule of pentane was located and disordered about a special position (inversion center), which could not be satisfactorily modelled without diffuse ellipsoids. The solvent molecule was squeezed out using the Olex2 mask function to improve the C–C bond precision. CCDC Identifier: 2049907.

Table S3. Pertinent bond metrics of (^{EMind}L)Cu(η^2-C_6H_6) (**1-benzene**).

Cu1–N1	1.997(2) Å	Σ (∠Cu1)	360.5(8) º
Cu1–N2	1.984(2) Å	∠N1–Cu1–N2	99.72(8) º
Cu1–C66	2.19(1) Å	Cu1–C67	2.24(2) º

Table S4. Pertinent bond metrics of (^{EMind}L)Cu(O_2) (**2**).

Cu1–N1	1.887(3) Å	Σ (∠Cu1)	360.0(2) º
Cu1–N2	1.885(3) Å	O1–O2	1.378(4) º
Cu1–O1	1.823(3) Å	Cu1–O2	1.834(3) º

Table S5. Pertinent bond metrics of (^{EMind}L)Cu(CH_2Cl_2) (**4**).

Cu1–N1	1.943(5) Å	Σ (∠Cu1)	359.7(5) º
Cu1–N2	1.949(5) Å	∠N1–Cu1–Cl1	118.4(3) º
Cu1–Cl1	2.177(9) Å	∠N2–Cu1–Cl1	141.7(3) º

Table S6. Pertinent bond metrics of (^{EMind}L)Cu(NH_2NH_2) (**5**).

Cu1–N1	1.955(3) Å	Σ (∠Cu1)	359.8(4) º
Cu1–N2	1.975(3) Å	∠N1–Cu1–N3	116.7(3) º
Cu1–N3	1.93(1) Å	∠N2–Cu1–N3	148.0(3) º
N3–N4	1.47(2) Å	∠ Cu1–N3–N4	117.2(8) º

Table S7. Pertinent bond metrics of (^{EMind}L)CuI (**6**).

Cu1–N1	1.913(6) Å	Σ (∠Cu1)	360.1(3) º
Cu1–N2	1.909(4) Å	∠N1–Cu1–I1	133.5(2) º
Cu1–I1	2.399(1) Å	∠N2–Cu1–I1	130.7(1) º

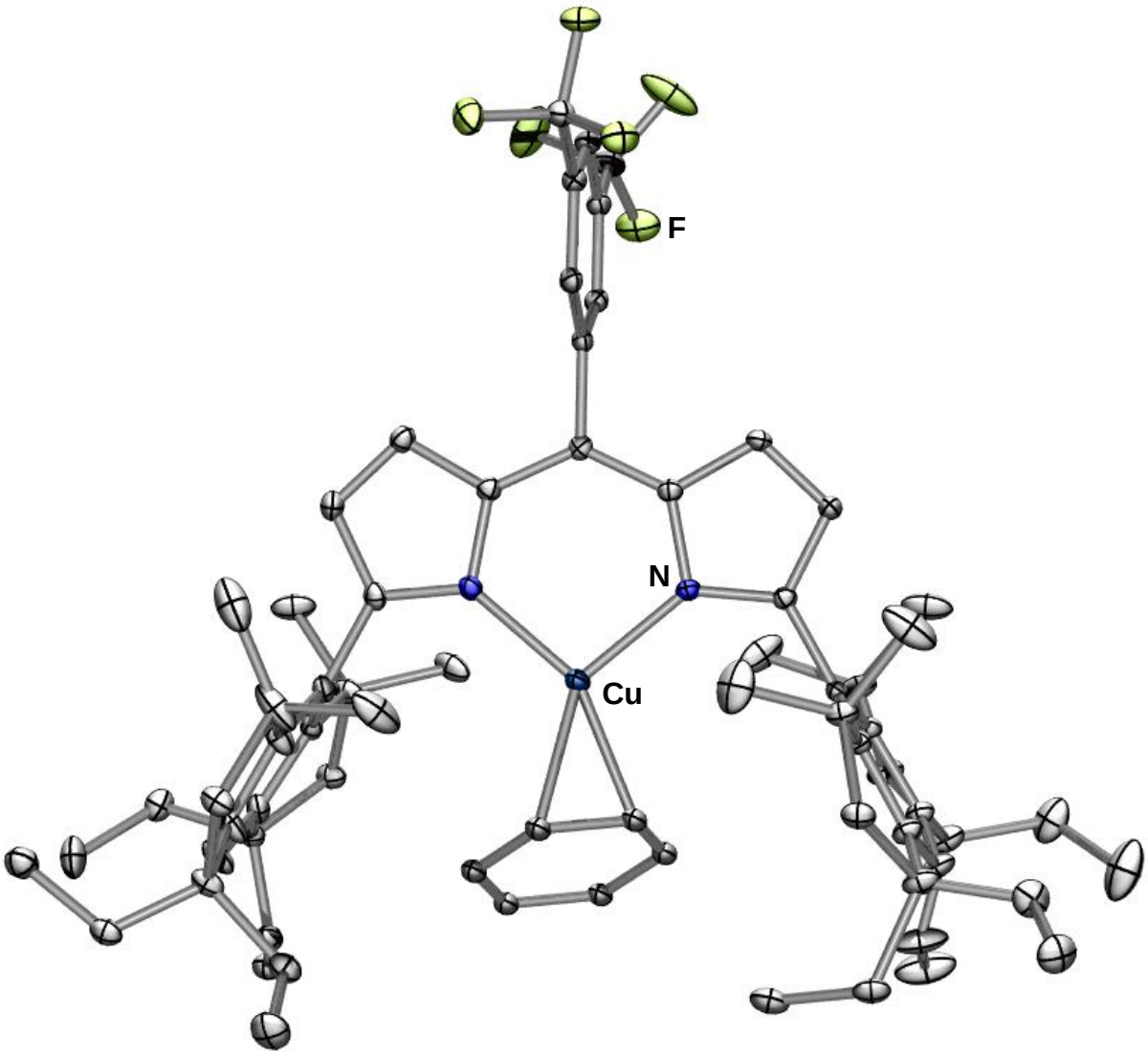

Figure S55. Solid-state molecular structure of (^{EMind}L)Cu(η^2-C_6H_6) with displacement ellipsoids at 50 % probability level. Hydrogen atoms, structural disorder, and solvent molecules are omitted for clarity. Color scheme: Cu (*cobalt blue*), F (*yellow-green*), N (*blue*).

Single crystals suitable for X-ray diffraction were obtained through reverse vapor diffusion of hexamethyldisiloxane into a saturated pentane solution of **1** with excess benzene (*ca*. 20 equiv.) under Ar. In the presence of N_2 and absence of excess benzene, reversion to (^{EMind}L)Cu(N_2) is observed in both solution and solid state.

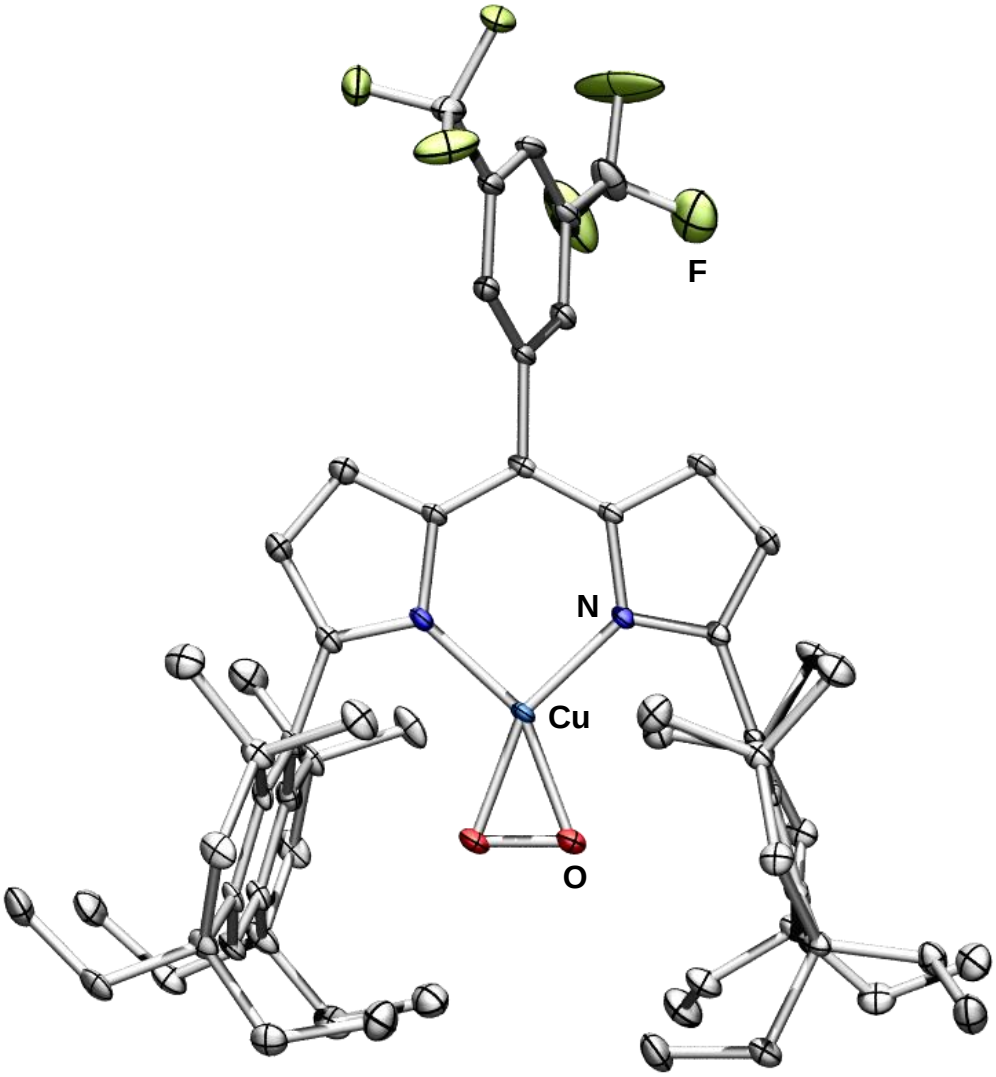

Figure S56. Solid-state molecular structure of (^{EMind}L)Cu(O_2) (**2**) with displacement ellipsoids at 50 % probability level. Hydrogen atoms, structural disorder, and solvent molecules are omitted for clarity. Color scheme: Cu (*cobalt blue*), F (*yellow-green*), N (*blue*), O (*red*).

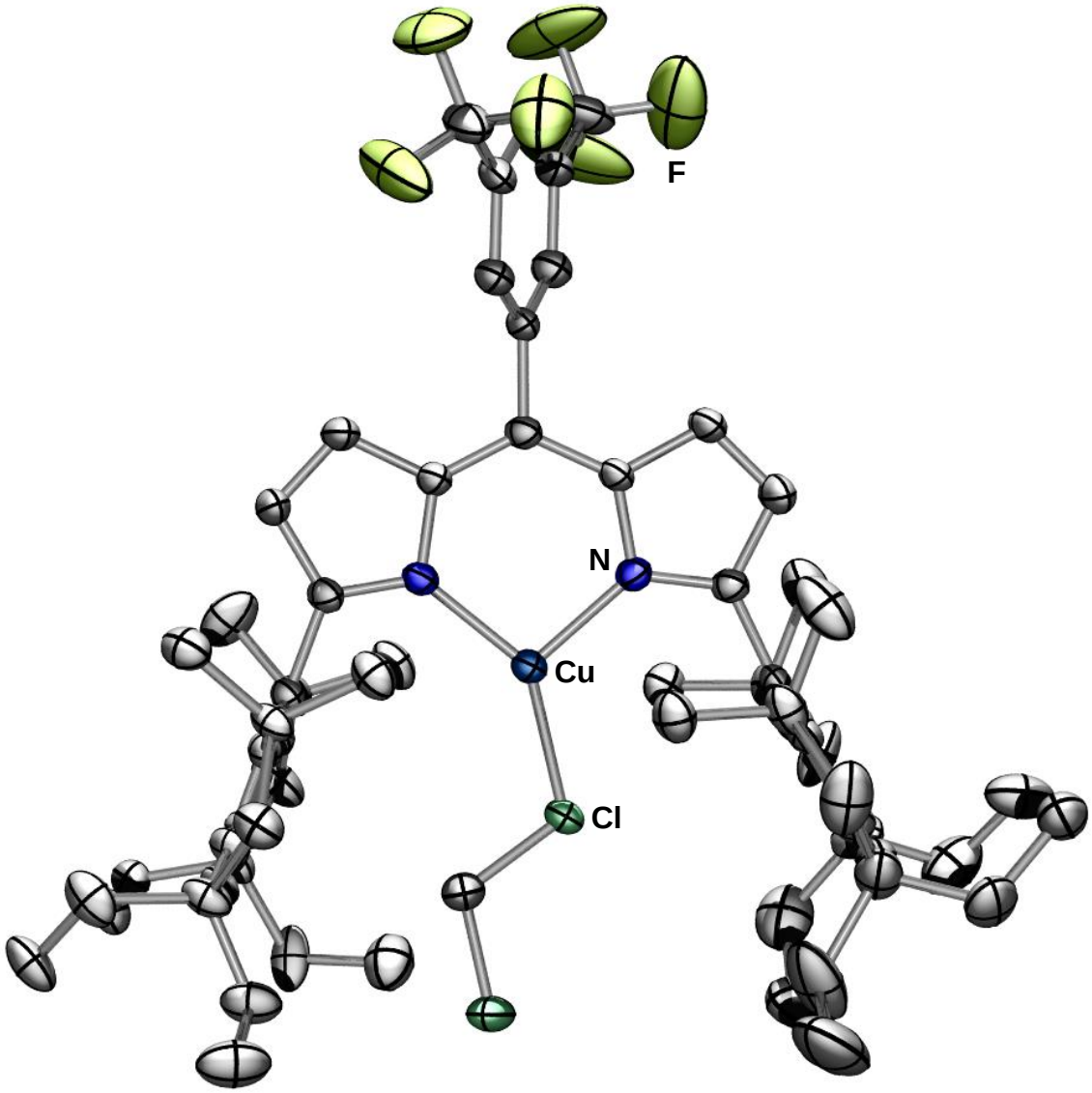

Figure S57. Solid-state molecular structure of (^{EMind}L)Cu(CH_2Cl_2) (**4**) with displacement ellipsoids at 50 % probability level. Hydrogen atoms, structural disorder, and solvent molecules are omitted for clarity. Color scheme: Cu (*cobalt blue*), Cl (*green*), F (*yellow-green*), N (*blue*).

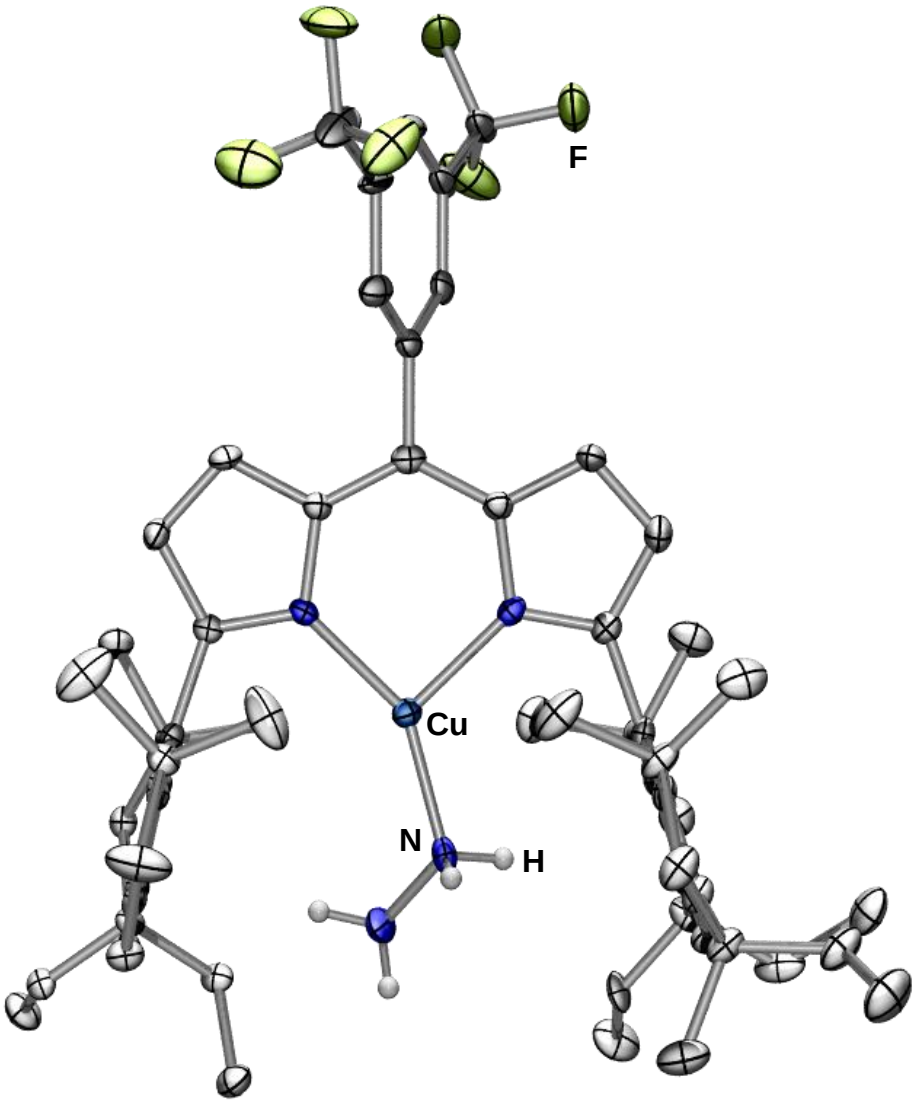

Figure S58. Solid-state molecular structure of (^{EMind}L)Cu(NH_2NH_2) (**5**) with displacement ellipsoids at 50 % probability level. Hydrogen atoms excluding those comprising the hydrazine fragment, structural disorder, and solvent molecules are omitted for clarity. Color scheme: Cu (*cobalt blue*), F (*yellow-green*), N (*blue*).

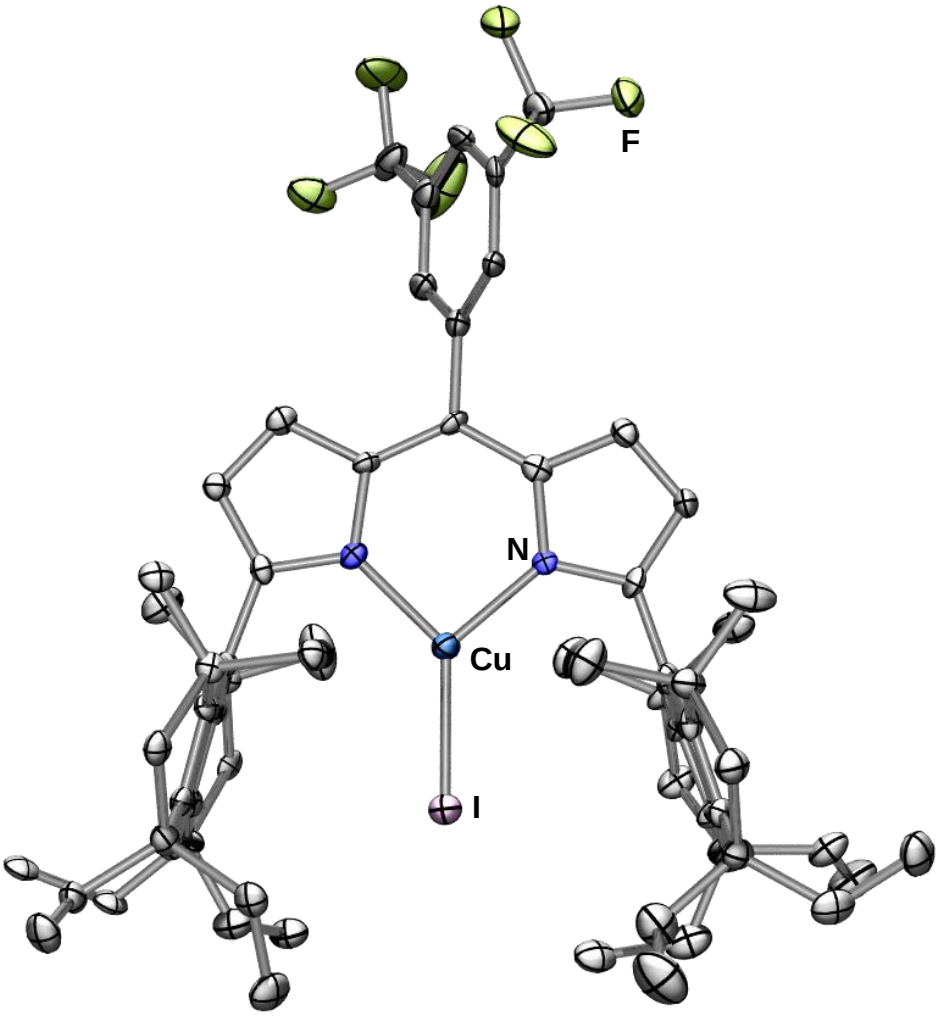

Figure S59. Solid-state molecular structure of (^{EMind}L)CuI (**6**) with displacement ellipsoids at 50 % probability level. Hydrogen atoms, structural disorder, and solvent molecules are omitted for clarity. Color scheme: Cu (*cobalt blue*), F (*yellow-green*), I (*pink*), N (*blue*).

References.

(1) Weitz, I. S.; Rabinovitz, M., The Application of C_8K for Organic Synthesis: Reduction of Substituted Naphthalenes. *J. Chem. Soc. Perkin 1* **1993**, 117.
(2) Kadassery, K. J.; Dey, S. K.; Cannella, A. F.; Surendhran, R.; Lacy, D. C., Photochemical Water-Splitting with Organomanganese Complexes. *Inorg. Chem.* **2017**, *56*, 9954.
(3) Konnick, M. M.; Guzei, I. A.; Stahl, S. S., Characterization of Peroxo and Hydroperoxo Intermediates in the Aerobic Oxidation of N-Heterocyclic-Carbene-Coordinated Palladium(0). *J. Am. Chem. Soc.* **2004**, *126*, 10212.
(4) Carsch, K. M.; DiMucci, I. M.; Iovan, D. A.; Li, A.; Zheng, S.-L.; Titus, C. J.; Lee, S. J.; Irwin, K. D.; Nordlund, D.; Lancaster, K. M.; Betley, T. A., Syntheses of a Copper-Supported Triplet Nitrene Complex Pertinent to Copper-Catalyzed Amination. *Science* **2019**, *365*, 1138.
(5) Stoll, S.; Schweiger, A., EasySpin, a Comprehensive Software Package for Spectral Simulation and Analysis in EPR. *J. Magn. Reson.* **2006**, *178*, 42.
(6) Francl, M. M.; Pietro, W. J.; Hehre, W. J.; Binkley, J. S.; Gordon, M. S.; DeFrees, D. J.; Pople, J. A., Self–Consistent Molecular Orbital Methods. XXIII. A Polarization–Type Basis Set for Second–Row Elements. *J. Chem. Phys.* **1982**, *77*, 3654.
(7) Hehre, W. J.; Ditchfield, R.; Pople, J. A., Self—Consistent Molecular Orbital Methods. XII. Further Extensions of Gaussian—Type Basis Sets for Use in Molecular Orbital Studies of Organic Molecules. *J. Chem. Phys.* **1972**, *56*, 2257.
(8) Grimme, S., Semiempirical Hybrid Density Functional with Perturbative Second-Order Correlation. *J. Chem. Phys.* **2006**, *124*, 034108.
(9) Becke, A. D., Density-Functional Thermochemistry. I. The Effect of the Exchange-Only Gradient Correction. *J. Chem. Phys.* **1992**, *96*, 2155.
(10) Barone, V.; Cossi, M., Quantum Calculation of Molecular Energies and Energy Gradients in Solution by a Conductor Solvent Model. *J. Phys. Chem. A* **1998**, *102*, 1995.
(11) Bochevarov, A. D.; Harder, E.; Hughes, T. F.; Greenwood, J. R.; Braden, D. A.; Philipp, D. M.; Rinaldo, D.; Halls, M. D.; Zhang, J.; Friesner, R. A., Jaguar: A High-Performance Quantum Chemistry Software Program with Strengths in Life and Materials Sciences. *Int. J. Quantum Chem.* **2013**, *113*, 2110.
(12) Busing, W. R.; Levy, H. A., Crystal and Molecular Structure of Hydrogen Peroxide: A Neutron-Diffraction Study. *J. Chem. Phys.* **1965**, *42*, 3054.
(13) Bruker AXS APEX3, Bruker AXS, Madison, Wisconsin, **2015**.
(14) Krause, L.; Herbst-Irmer, R.; Sheldrick, G. M.; Stalke, D., Comparison of Silver and Molybdenum Microfocus X-Ray Sources for Single-Crystal Structure Determination. *J. Appl. Crystallogr.* **2015**, *48*, 3.
(15) Sheldrick, G., SHELXT – Integrated Space-Group and Crystal-Structure Determination. *Acta Crystallogr. A* **2015**, *71*, 3.
(16) Sheldrick, G., Crystal Structure Refinement with Shelxl. *Acta Crystallogr. C* **2015**, *71*, 3.
(17) Dolomanov, O. V.; Bourhis, L. J.; Gildea, R. J.; Howard, J. A. K.; Puschmann, H., Olex2: A Complete Structure Solution, Refinement and Analysis Program. *J. Appl. Crystallogr.* **2009**, *42*, 339.
(18) Spek, A., Single-Crystal Structure Validation with the Program PLATON. *J. Appl. Crystallogr.* **2003**, *36*, 7.
(19) Ramadhar, T. R.; Zheng, S.-L.; Chen, Y.-S.; Clardy, J., Analysis of Rapidly Synthesized Guest-Filled Porous Complexes with Synchrotron Radiation: Practical Guidelines for the Crystalline Sponge Method. *Acta Crystallogr. A* **2015**, *71*, 46.

(20) Persistence of Vision Raytracer. *http://www.povray.org/*.